Linac-Ring eRHIC.

Daniel Anderson, Ilan Ben-Zvi[1], Rama Calaga[1], Xiangyun Chang[1], Manouchehr Farkhondeh[2], Alexei Fedotov[1], Jörg Kewisch[1], Vladimir Litvinenko[1], William Mackay[1], Christoph Montag[1], Thomas Roser[1], Vitaly Yakimenko[3]

[(1)] C-AD, BNL [(2)] Bates, MIT [(3)] Physics Department, BNL

Content **page**

1. Introduction to the Linac-Ring collider

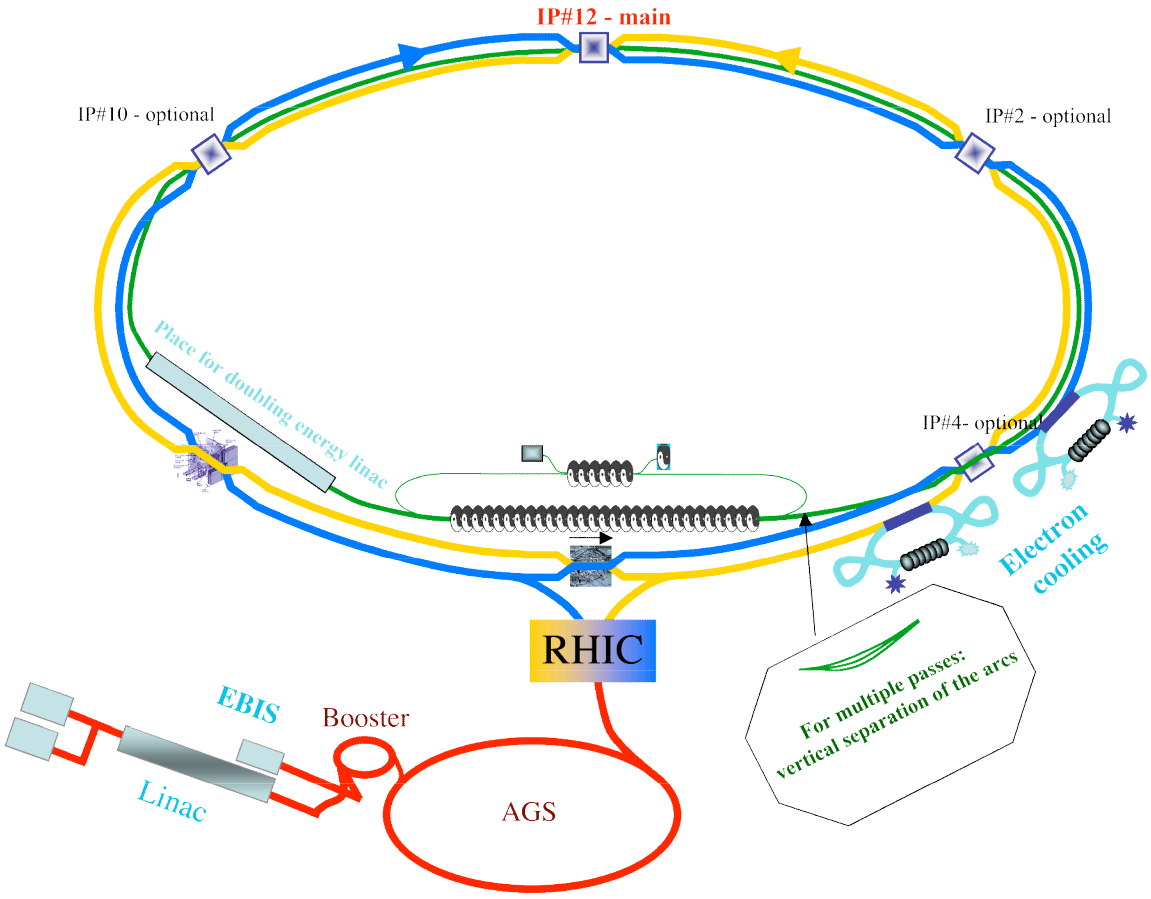

Figure 1.1.a. The most natural linac-ring eRHIC with multiple IP(s) with the arcs are located in the RHIC tunnel. A polarized electron beam generated in a photo-injector is accelerated to the energy of the experiment in the ERL. After colliding with the hadron RHIC beam in as many as four IP(s), the electron beam is decelerated to energy of few MeV and damped. The energy thus recovered is used for accelerating subsequent bunches to the energy of the experiment. Electrons by-pass both the Star and Phenix experimental halls. The main 5 GeV superconducting linac, which electron beam passes twice during acceleration and twice during deceleration, the injection and the beam damp are located north of the Star experimental hall. The by-pass around the Phenix experimental hall is the natural place for a future linac, which extends the electron beam energy to and above 20 GeV *(see section 6 for detail)*.

The Linac-Ring eRHIC has a large number of unique features, which make it a perfect match for versatile nuclear physics program at Brookhaven National Laboratory by:

- ✓ providing luminosity up to 10^{34} cm^{-2} s^{-1} in electron-hadron collisions [1];
- ✓ providing full polarization transparency at all energies [2] ;
- ✓ providing multiple electron-hadron interaction points (IPs) and detectors [3];
- ✓ providing very long "element-free" straight section(s) for detector(s);
- ✓ taking full advantage of electron cooling of the RHIC II hadron beams;
- ✓ being perfectly compatible with RHIC operations and hadron-hadron collisions[4];
- ✓ providing full range of C-M energies required for the physics program;
- ✓ being directly upgradeable to electron energies of 20 GeV and above.

The choices of the IPs or/and the exact layout of the electron accelerator in the linac-ring configuration are completely flexible. Figures 1.1 a,b and c give a flavor of possible schematic layouts of the Linac-Ring $\vec{e} \square \vec{p}$ and e-Au^{79}_{197} collider based on an energy-recovery linac (ERL) and the RHIC facility. These figures *are not drawn to scale*.

In all these schemes a high-brightness polarized electron beam generated in a photo-injector is accelerated to the energy of experiment 2 GeV – 10 GeV (*and possibly to 20+ GeV in future*) in the super-conducting energy recovery linac (ERL). After the collision(s) with proton/ion beam in the IP(s), the electron beam is decelerated to energy of few MeV in the same ERL and damped. By this process the energy of the electrons is recovered and is used for accelerating subsequent bunches to the collision point.

The simple fact that linac-ring eRHIC uses fresh electron beam for each collision is of the foremost significance for all attractive features of this scheme. Most importantly, the use of fresh beam removes the tune shift limit on electron beam and opens the range of collider parameter-space inaccessible by ring-ring scheme. As the result, the linac-ring eRHIC provides for higher luminosity at any given level of RHIC performance, compared with the ring-ring case. This scheme meets or exceeds the requirements for the collider specified in the physics program for eRHIC [1]:

- ✓ Electron beams colliding with beams of protons or light and heavy nuclei
- ✓ Wide range of collision energies (E_{cm}/nucleon from 15 GeV to 100 GeV)
- ✓ High luminosity L > 10^{33} cm^{-2} s^{-1} per nucleon
- ✓ Polarization of electron and proton spins
- ✓ Preferably, two interaction regions with dedicated detectors.

---

[1] Luminosity is quoted $\vec{e} \square \vec{p}$ collisions. This number is also correct for e - Au^{79}_{197} , when luminosity is calculated *per nucleon*. Quoted luminosity assumes that eRHIC runs in a dedicated mode – see discussion below.

[2] In contrast with ring-ring option, the linac-ring eRHIC does not have prohibited energies where beam polarization vanishes.

[3] In the case of multiple IPs, the total luminosity is ~ 10^{34} cm^{-2} s^{-1}

[4] In this mode of operation the eRHIC luminosity will be limited by a total beam-beam tune shift for hadron beam, i.e. to a portion of 10^{34} cm^{-2} s^{-1}.

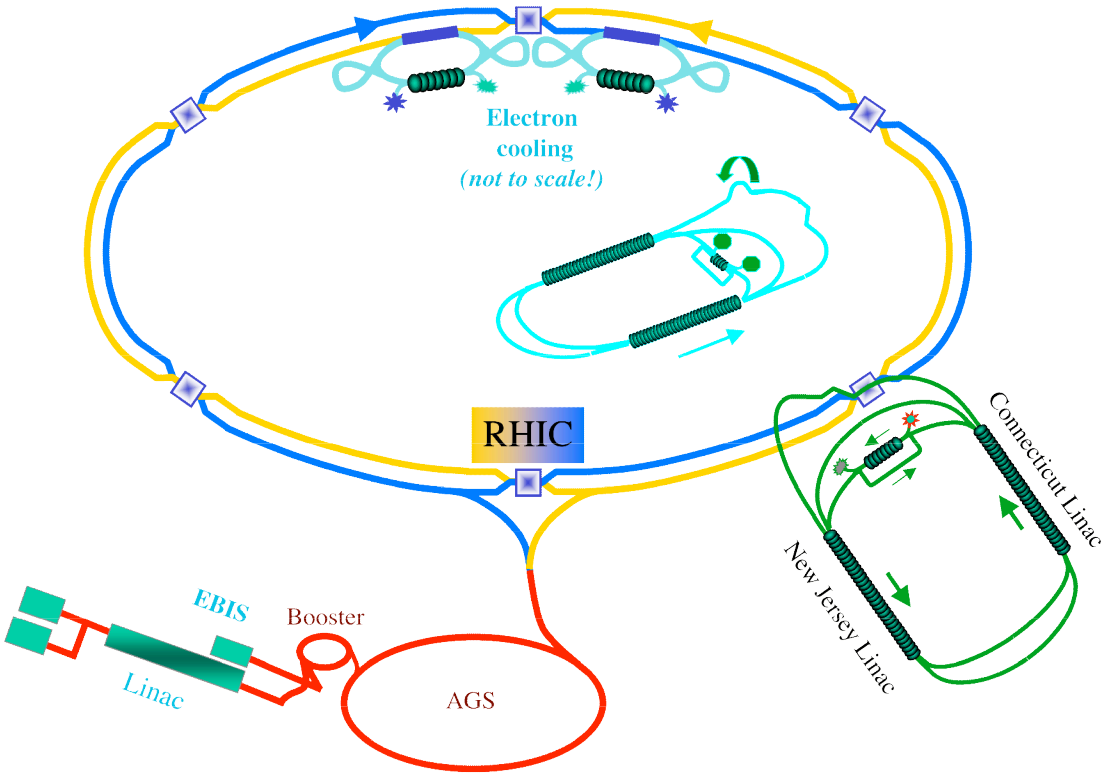

Figure 1.1.b. Linac-ring eRHIC with a separate tunnel and an IP at 4 o'clock. A polarized electron beam generated in a photo-injector is accelerated to the energy of the experiment in the ERL. After colliding with the hadron RHIC beam in the IP, the electron beam crosses over both blue and yellow RHIC rings and is decelerated to energy of few MeV in the same ERL and damped. The energy thus recovered is used for accelerating subsequent bunches to the energy of the experiment. Both Blue and Yellow ring (hence the colors of the lines) of the RHIC as well its injector (red lines) operate in standard conditions for hadron collisions, while the electrons (green lines) collide with hadron beam in the Yellow ring at 4 o'clock. Both hadron beams are cooled by electron beam coolers (light blue lines) located at 12 o'clock. Note, that both electron cooling and ERL can be relocated to an IP at 10, 12 and 2 o'clock.

The first feature *(Electron beams colliding with beams of protons or light and heavy nuclei)* is satisfied by having a variety of nuclei (*p, D, Au, He*…) accelerated by the blue and yellow ring of the RHIC, and by ERL's polarized e-beam with continuously tunable energy.

The ERL-based eRHIC has very large tunability range of c.m. energies while maintaining very high luminosity (*14.4 - 100 GeV per nucleon in e-p collisions and 20 - 63 GeV in e-Au collisions – see Tables 1.1 and 1.2 for details; the possibilities of extending this range further are discussed in chapter 6*).

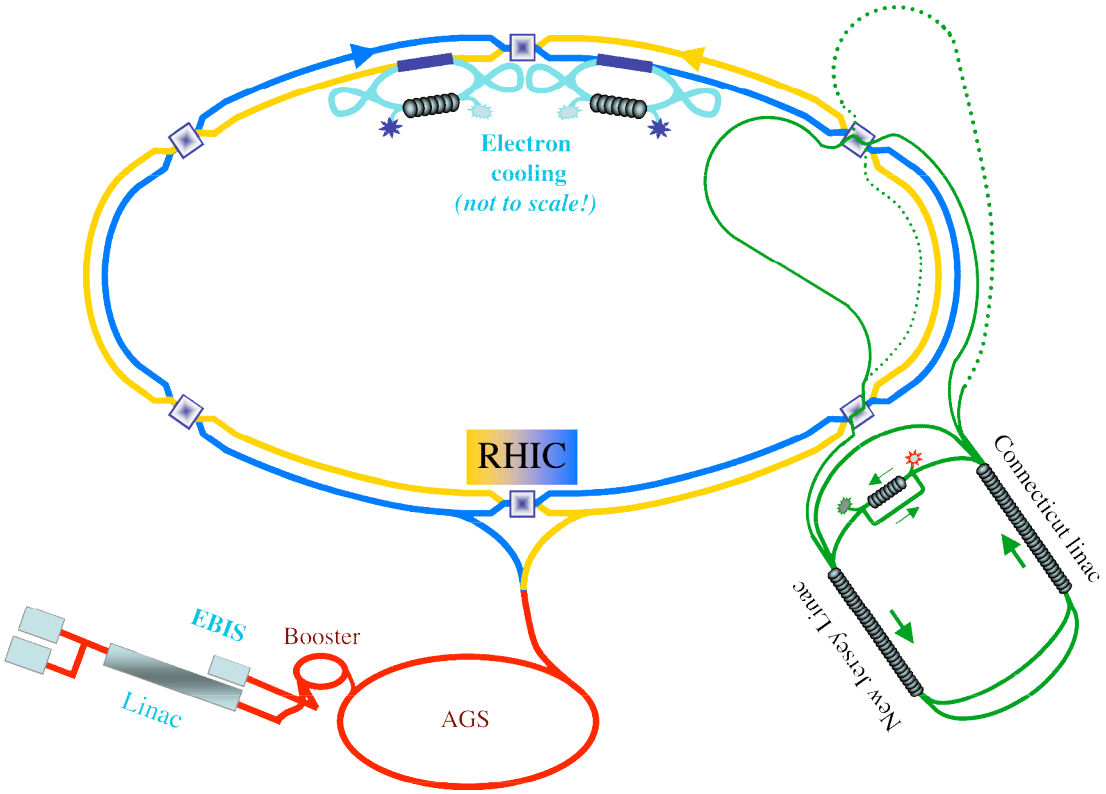

Figure 1.1.c. eRHIC (based on stand-along ERL) with two IPs.

Table 1.1 Center of mass energy per nucleon (GeV, green) in *e-p* collisions in eRHIC vs. energy of protons (red) and ERL (blue)

Energy, GeV **proton** **electrons** c.m.	**26**	**50**	**100**	**250**
2	**14.42**	20.00	28.28	44.72
5	22.80	31.62	44.72	70.71
10	32.25	44.72	63.25	**100.00**

Table 1.2 Center of mass energy per nucleon (GeV, green) in e - $^{79}Au_{197}$ collisions in eRHIC vs. energy of ions per nucleon (red) and ERL (blue)

Energy, GeV **Au/u** **e** c.m.	**50**	**100**
2	**20.00**	28.28
5	31.62	44.72
10	44.72	**63.25**

In the ERL-based eRHIC we collide two round beams of equal size (see section 3.f) to maximize the luminosity. The main distinctive feature here is that the attainable luminosity is defined in practice by the energy and intensity of the proton or ion beam in RHIC:

$$L = f_c \cdot \square_h \cdot \frac{\square_h}{\square_h^*} \cdot \frac{Z \cdot N_h}{r_h} \tag{1}$$

i.e., by the intensity N_h (number of hadrons per bunch), repetition rate f_c, the energy of the ion or proton beam, $\square_h = E_h / Mc^2$, its charge $q = Ze$, its classical radius $r_h = Z^2 e^2 / Mc^2$, and the allowable beam-beam tune shift $\square_h$ in the eRHIC IP(s) (*see explanation in the next section*). The linac-ring eRHIC's luminosity is independent of the electron beam's energy and linearly proportional to the energy of the proton or ion beam. This means that that the same center of mass energy, (*given that there is no preferred energy ratio*), can be reached using higher energy protons (ions) and lower energy electrons; hence, the high luminosity.

There are two possible modes of eRHIC operation:

a) A parallel with the normal RHIC collider where hadrons are colliding with hadrons in 2 detectors. This mode is considered to be typical for eRHIC;

b) A dedicated mode when hadrons collide only with electrons.

In any mode of operation, the total allowable beam-beam tune shift for hardons in RHIC is limited to $\sum_{IPs} \square_h \square 0.024$ [2]. It is considered that with three beam-beam interaction points, two for hadron-hadron and one for electron-hadron collisions, the beam-beam parameter per interaction point should not exceed $\square_h = 0.007$ [3]. The hadron beam-beam tune shift in the linac-ring eRHIC IP is given by following formula:

$$\square_h = \frac{N_e}{\square_h} \cdot \frac{r_h / Z}{4\square\square_h} \tag{2}$$

where N_e is number of electrons per bunch and $\square_h$ RMS emittance of hadron beam. Therefore, for a given energy and species hadron beam and for given intensity of electron beam in ERL we will control the hadron beam-beam parameter by changing the hadron beam emittance via electron cooling [5] (see section 3.e). This is an additional advantage of the linac-ring eRHIC – the betterment of electron cooling allows the reduction of the hadron beam emittance with a proportional reduction of the electron beam intensity (and the related to it synchrotron radiation back-ground in the detectors) while keeping the luminosity (1) constant.

The other parameter which influence the eRHIC luminosity is the hadron beam intensity:

$$I_h = Ze \cdot f_c \cdot N_h . \tag{3}$$

[5] We plan to cool gold ions energy of operation, while pre-cool protons at energy of 27 GeV before accelerating them to 250 GeV – see section 3.e.

The number of hadrons per bunch is limited by the single bunch stability [4]. With present parameters of RHIC, the hadron bunches with intensities following intensities will be stable [4]:

□h	Species	Threshold, same □Q
250	Protons	4.3e11
107	Gold	5.8e9

The collision rep-rate is determined by the revolution frequency $f_o \square 78\ kHz$ and number of hadron bunches in RHIC N_b:

$$f_c = f_o \cdot N_b .$$

Presently RHIC operates up to 60 bunches with $N_p \sim 10^{11}$, $N_{Au} \sim 10^9$ per bunch. Doubling the number of hadron bunches to 120 while keeping the bunch intensity at present level is considered as the main stream goal for RHIC II luminosity up-grade, which employs electron cooling of hadron beams [2]. The hadron beam parameters RHIC II are considered to be realistic and should reached many years before commissioning of the eRHIC.

The ring-ring eRHIC requires 6-fold increase of the hadron beam intensity compared with the present level of performance of RHIC. Specifically [3], it suggests using 360 hadron bunches in RHIC for eRHIC operation. The intensity of the hadron beam can be limited by a number of factors such as development of electron cloud or by exceeding the cryogenic load in the RHIC super-conducting magnets, to mention few. These issues as well as their technical and financial implications for RHIC require further detailed studies.

For simplicity, we show here the linac-ring eRHIC luminosities two cases:

- the most optimistic:
  - 360 bunches (as in ring-ring case [3]) with $N_p = 2 \cdot 10^{11}$, $N_{Au} = 2.5 \cdot 10^9$ per bunch;
- the most realistic [6]:
  - 120 bunches (as in RHIC II) with $N_p \sim 10^{11}$, $N_{Au} \sim 10^9$ per bunch.

The maximum luminosity of the linac-ring eRHIC for both the proton-electron and the gold-electron collisions is given in Tables 1.3 and 1.4. Note that luminosities at the level of **10^{34} cm^{-2}sec^{-1}** per nucleon can be reached in linac-ring eRHIC independently from the energy of electrons used. The ratio of luminosity between the parallel and dedicated modes of operation is approximately 3.4.

[6] 120 bunch mode was tested at RHIC but with reduced intensity per bunch. Note using 120 bunches instead of 360 reduces luminosity by a factor of 3 for both linac-ring and ring-ring eRHIC.

Table 1.3 Luminosities for e-p collisions for various energies *in the ERL- based eRHIC: 360 bunches with* $2 \cdot 10^{11}$ *protons per bunch.*

Luminosity 10^{33} **cm**$^{-2}$**sec**$^{-1}$	*Protons 26 GeV*	*Protons 50 GeV*	*Protons 100 GeV*	**Protons 250 GeV**
Parallel mode	**0.285**	**0.548**	**1.097**	**2.74**
Dedicated mode	**0.978**	**1.88**	**3.76**	**9.40**

Table 1.4 Luminosities for e-Au collisions for various energies *in the ERL- based eRHIC*: *360 bunches with* $2.5 \cdot 10^{9}$ *gold-ions per bunch.*

Luminosity (per nucleus) 10^{31} **cm**$^{-2}$**sec**$^{-1}$	*Au 50 GeV/u*	*Au 100 GeV/u*
Parallel mode	**1.71**	**3.42**
Dedicated mode	**5.86**	**11.7**

What is quite remarkable, is that the linac-ring eRHIC can reach luminosities at the level of **10^{33} cm^{-2}sec^{-1}** per nucleon with beam parameters which are currently attainable at RHIC: 120 bunches with intensities of $Z \cdot N_h \sim 10^{11}$. These parameters are shown in Table 1.5 and Table 1.6.

Table 1.5 Luminosities for e-p collisions with intensities of proton beam for RHIC II: *120 bunches with* 10^{11} *protons per bunch.*

Luminosity 10^{33} cm^{-2}sec^{-1}	*Protons 26 GeV*	*Protons 50 GeV*	*Protons 100 GeV*	Protons 250 GeV
Parallel mode	.0456	0.0914	0.183	0.457
Dedicated mode	0.156	0.313	0.627	1.57

Table 1.6 Luminosities for e-p collisions with intensities of gold-ion beam for RHIC II*: 120 bunches with 10^9 ions per bunch..*

Luminosity (per nucleus) 10^{31} $cm^{-2}sec^{-1}$	*Au* *50 GeV/u*	*Au* *100 GeV/u*
Parallel mode	0.228	0.456
Dedicated mode	0.781	1.56

It worth noting that eRHIC parameters in the last two tables are reachable with one third of the electron beam current required for ring-ring operations and, therefore, one third of the back-ground from the synchrotron radiation in the detectors.

Overall, the eRHIC based on the emerging technology of superconducting RF ERL promises to deliver the extremely high luminosity required for the eRHIC physics program. It will also provide several very important features that are not possible or likely impossible with other collider technologies.

1.1 Advantages of the ERL-based eRHIC

- Usage of a fresh electron beam and absence of the memory in the e-beam
  - waives in practice the limitation on the tune shift in the IP, and
    - increase in the density of the proton/ion beam
    - **10 fold increase in the luminosity**
    - larger β_e^* for the e-beam and simplified IP geometry
      - smaller e-beam emittance
      - smaller angular divergence in IP
      - smaller aperture for e-beam
      - **no-need for e-beam quads in the detector area**
      - possibility of focusing the e-beam after separating it for protons/ions
      - **simplified IP geometry**
  - reduces the number of coupled-bunch instability modes
  - secures spin-transparency of the system at all energies
  - provides a high (80%+) degree of e-beam polarization at all energies
  - eliminates "prohibited" energies for the e-beam
  - precludes the need to preserve beam qualities (polarization, emittance…) after the IP(s)
    - simple geometry of the return pass
    - absence of spin-resonances
    - possible multiple collisions (IPs)
- Usage of the linac (ERL) geometry
  - ensures easy adjustment the e-beam repetition rate to that of the beam in the RHIC, which significantly depends on the ion energy (equivalent change in circumference is ~ 30m);
  - allows straightforward upgrades of the e-beam's energy
  - opens possibility of using multiple energy collisions
  - offers possibility of employing an γ-ion collider with an ERL-based Compton source of γ-rays

There are some limitations for ERL-based eRHIC that include

- No positron-ion collisions;
- Need for intense R&D program on
  - High-intensity, high-current polarized electron source
  - High current ERLs

[1] "The Electron Ion Collider", A white paper summarizing the scientific opportunities and the preliminary detector and accelerator design options, February 2002, http://www.phenix.bnl.gov/WWW/publish/abhay/Home_of_EIC/Whitepaper/Final/

[2] "Upgrading RHIC for Higher Luminosity", W. MacKay, I. Ben-Zvi, J.M. Brennan, M. Harrison, J. Kewisch, S. Peggs, T. Roser, D. Trbojevic, V. Parkhomchuk, Proc. Of PAC'2001, Chicago, Illinois U.S.A. June 18-22, 2001

[3] General accelerator concept and parameters, V.Ptitsyn, T.Roser, F.Wang, eRHIC ZDR, Chapter 1.1, http://www.agsrhichome.bnl.gov/eRHIC/eRHIC_ZDR.htm

[4] "Instabilities in RHIC", M.Blaskiewicz, W. Fischer, eRHIC ZDR, Chapter 3.2.5, http://www.agsrhichome.bnl.gov/eRHIC/eRHIC_ZDR.htm

2. Main beam parameters and Luminosity

In contrast with ring-ring eRHIC [3], the IP of the ERL-based eRHIC has round beam geometry in the IP (i.e., *its horizontal and vertical emittances as well as β* are equal*), which is optimal for attaining maximum luminosity. The sizes of the electron and hadron beams are chosen to be equal

$$\varepsilon_e^* \varepsilon_e = \varepsilon_h^* \varepsilon_h \tag{2.1}$$

by selecting β^* of the electron beam to be $\beta_e^* = \beta_h^* \varepsilon_h / \varepsilon_e$.

For operating the ERL-based eRHIC, we propose using the same number of hadron bunches (360 bunches, rep-rate ~28 MHz) in the RHIC-ring as in the main part of the ZDR [2.1]. Because of the lifting of limitations on the electron beam's tune shift in the ERL case, the number of hadrons per bunch is set to the present limit in RHIC: $2 \cdot 10^{11}$ of protons or $2 \cdot 10^9$ gold-ions.

Table 2.1. Main parameters of the beams and the IP in ERL-based eRHIC.

RHIC	
Ring circumference [m]	3834
Number of bunches	120-360
Beam rep-rate [MHz]	28.15
Protons:	
Beam energy [GeV]	26 - 250
Protons per bunch	$1.0 - 2.0 \cdot 10^{11}$
Normalized 96% emittance [μm]	4-14.5
β^* [m]	0.26
RMS Bunch length [m]	0.2
Beam-beam tune shift in eRHIC	0.005
Synchrotron tune, Qs	0.0028 (see [2.4])
Gold ions:	
Beam energy [GeV/u]	50 - 100
Ions per bunch (max)	$1.0 - 2.5 \cdot 10^9$
Normalized 96% emittance [μm]	1.5-6
β^* [m]	0.25
RMS Bunch length [m]	0.2
Beam-beam tune shift	0.005
Synchrotron tune, Qs	0.0026
Electrons:	
Beam rep-rate [MHz]	9.38 - 28.15
Beam energy [GeV]	2 - 10
RMS normalized emittance [μm]	1- 50 *for $N_e = 10^{10}$ / 10^{11} e^- per bunch*
β^* [m]	0.3-1m, *to fit beam-size of hadron beam*
RMS Bunch length [m]	0.01
Electrons per bunch	$0.1 - 1.0 \cdot 10^{11}$
Charge per bunch [nC]	1.6 – 16*(see below)*
Average e-beam current [A]	0.015 – 0.45

The intensity of the electron beam is limited by the allowable tune shift for hadrons in the eRHIC IP:

$$\Delta_h = \frac{N_e}{\gamma_h}\frac{\beta_h^*}{4\pi}\cdot\frac{r_h/Z}{\varepsilon_e^*\beta_e^*} \quad .$$

With the matching condition present (2.1), it obtains a simpler form that depends only on the number of electrons and the hadron beam's parameters:

$$\varepsilon_e^*\beta_e^* = \varepsilon_h^*\beta_h^* \quad \Rightarrow \quad \Delta_h = \frac{N_e}{\gamma_h}\frac{r_h}{4\pi Z\varepsilon_h} \tag{2.2}$$

Thus, limit for the hadron tune shift (2.2) limits the number of electron per bunch to

$$N_e = \gamma_h\cdot\Delta_{h\ \max}\cdot\frac{4\pi Z\varepsilon_h}{r_h} \quad \approx 1\cdot 10^{11} \quad \text{for 250 GeV p \& 100 GeV/u Au ions} \tag{2.3}$$

In this document we consider that condition (2.2) is satisfied and the hadron beam is stable under such collisions.

- **Luminosity limitations**

For round beam geometry with equal beam sizes, the luminosity formula is very simple :

$$L = f_c\frac{N_e N_h}{4\pi\varepsilon_h^*\beta_h^*}. \tag{2.4}$$

where f_c is the collision repetition rate.

The strongest limitation of eRHIC luminosity in the linac/ring configuration arises from the limitation on the beam-beam tune shift for hadrons (2.2):

$$L = f_c\cdot\gamma_h\cdot N_h\cdot\frac{\Delta_h\cdot Z_h}{\beta_h^*\cdot r_h}, \tag{2.5}$$

that defines the dependence of maximum attainable luminosity through the hadron beam's parameters. It worth noting that the maximum attainable luminosity is directly proportional to the energy of hadron (ion) beam. For the linac-ring collider, the beam-beam effect on the electron beam is better described not by a tune shift but by a disruption parameter:

$$D = \frac{Z_h N_h}{\gamma_e}\frac{r_e}{\sigma^2_{r(h)}}\sigma_{s(h)}$$

Our studies of the electron beam dynamics in the IP (see section 3.f.2) showed that disruption parameters (attainable within parameter-range in Table 2.1) do not limit the eRHIC luminosity. In the ERL configuration, the growth of the beam's emittance in the IP is acceptable for full energy recovery. Thus for, for the parameters listed in Table 2.1, the ERL operation will be stable.

An additional limitation on luminosity may come from the so-called "kink hard head-tail" instability, i.e., the transverse coupled mode instability of ion beam [2.2]. This effect is similar for the linac-ring and for the ring-ring collisions: the head of hadron

bunch can affect its tail by altering the position of the electron beam propagating through the ion beam in the IP. According to a rather conservative analysis[7] [2.3], the beams are stable when

$$\Xi = \frac{D \cdot \Phi_h}{Q_s} < 2\Pi. \qquad (2.6)$$

This stability criterion is satisfied for the most[8], but not all, of the parameter range we did considered above. The stability criteria (2.6) can be exceed in parallel mode of operation for electron energies below 5 GeV as well as for 10 GeV electrons in the dedicated mode of eRHIC operation.

We plan to use a simple feedback system for stabilizing this potential instability. The idea of the feedback is based on the fact that electron bunches are very short (~ 1 cm) and do oscillate a whole in the kink-instability. Thus, using a detector of the transverse position of the electron beam after the IP and applying the transverse kick to a fresh electron bunch, which will interact with the same hadron bunch on a consecutive turn about the RHIC, will suppress the instability. This feedback system, requiring a very decent bandwidth ~ 56 MHz, has many precedents in the accelerator technology. Again, the use of fresh electron bunch for the ERL makes the concept of the feedback very straight-forward and transparent.

- **Luminosity constraints**

Other luminosity constraints can come from the limitation of the detector's DAQ-speed or from the background created by synchrotron radiation from the electron beam. The latter is very unlikely to occur in the linac-ring version of eRHIC. Using a low emittance electron beam and a large β_e^* in the linac-ring version of eRHIC very significantly reduces the angular spread of the synchrotron radiation (8-to-10 fold vertically), which can leave the interaction region with relative ease (see section 3.f for details).

References:

[2.1] ZDR's section 1.2: V.Ptitsyn, General accelerator concept and parameters http://www.agsrhichome.bnl.gov/eRHIC/

[2.2] R.Li, B.C.Yunn, V.Lebedev, J.J.Bisognano, Proceedings of PAC 2001 (2001) p.2014

E.A. Perevedentsev, A.A.Valishev, Phys. Rev. ST-AB **4**, 024403 (2001)

[2.3] R.Li, B.C.Yunn, ICFA Beam Dynamics Newsletter No. 30, April 2003, p.69

[2.4] Synchrotron frequencies are taken from Instability limit on ion bunch length, M.Blaskiewicz, eRHIC, Meeting: July 15, 2003www.agsrhichome.bnl.gov/eRHIC/

[7] This analysis does not take into account the tune spread induced in the ions at the IP. It is known that tune spread can cause Landau damping and, hence, large stability range of the beams. Simple arguments of the phase mixing lead to a slightly different stability criteria $D < 2\Pi$.

[8] A 10 GeV electron beam colliding with 2 10^9 Au ions in parallel mode gives $\Pi = 3.5$, and a 10 GeV electron beam colliding with 2 10^{11} proton in parallel mode gives $\Pi = 4.09$.

3. Layout of the linac-ring eRHIC

Main components of the ling-ring eRHIC are show in the following figure:(one of several possible configurations – not in scale, see layouts in the Section 1.)

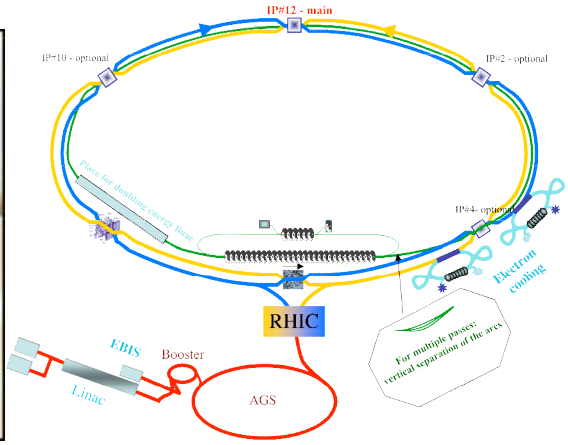

- RHIC – remains practically unchanged with exception of one IP http://www.bnl.gov/RHIC
- Electron cooling – as described in section 3.e

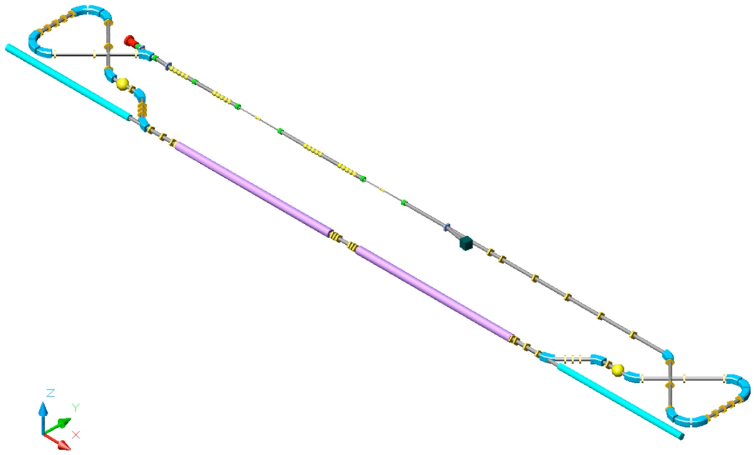

- Polarized electron gun - – as described in sections 3b and 3c
- Accelerating super-conducting linacs – see following section

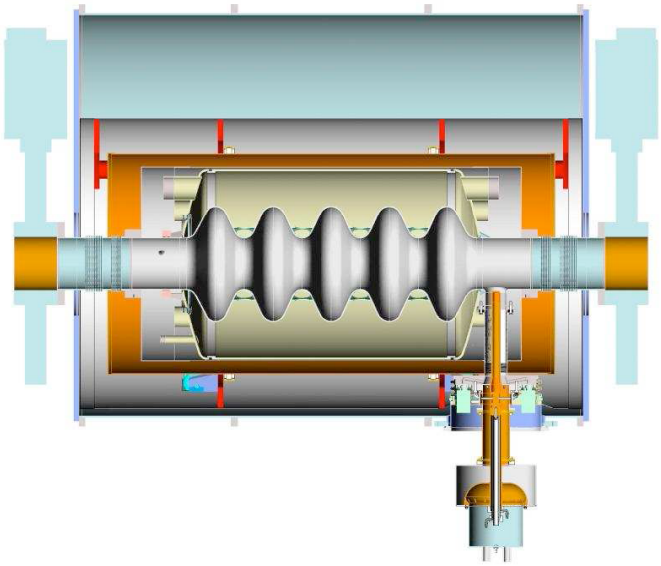

- Arcs and turns – The ERL has four major and two minor arcs. Arcs are comprised of a rather simple FODO lattice with high density, but low field dipoles (for reducing synchrotron radiation losses to about 5 MeV for the entire cycle from the gun to the damp). The arc with the largest energy of electrons incorporates the IP. Issues related to spin transparency are described in section 3.d.
- Interaction region – see section 3.f
- Returning pass and beam dump – It is not necessary to preserve the high quality of the e-beam and its polarization after the collision. Accordingly, a returning half-arc can be designed after the IP with a vertical chicane for avoiding a second crossing with the RHIC rings (see section 2.2 and 2.5 in the main part of ZDR). The returning pass serves the rather *simple but critical role* of recovering energy from the decelerating beam into the superconducting RF system. With the exception of the first half-arc, the decelerating beam reuses the same arcs. Finally, at the end of the deceleration process, the electron beam's residual energy, which is well below 10 MeV, is damped. Using damping energy below 10 MeV is a very critical environmental issue – it avoids residual radioactivity in the damp.

The following additional major systems are required for the linac-ring eRHIC, but are not shown in the above schematic:

- $2K^{o}$ helium refrigerator for superconducting RF cavities
- 700 MHz RF power system
- Power supplies for ERL's and arc's magnets
- Auxiliary RF system for compensating synchrotron radiation losses

3.a Energy recovery linac

Figure 3.a.1.is a schematic of the proposed two-stage 10-GeV energy-recovery linac based on 703.75 MHz super-conducting RF-linacs for the eRHIC.

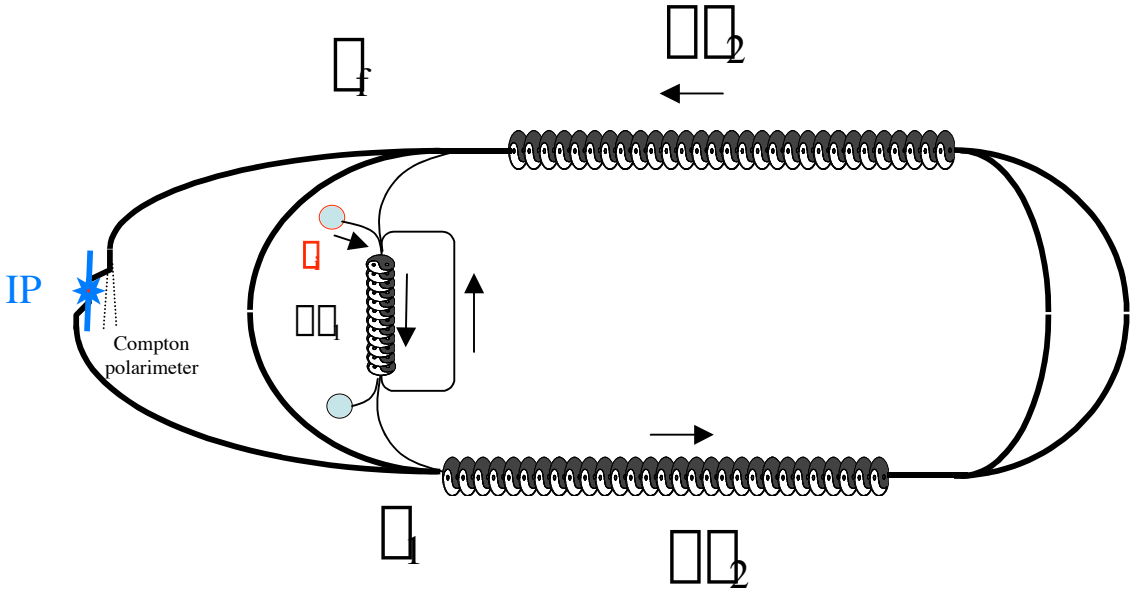

Fig. 3.a.1 Schematic of the two-stage ERL.

In this section we give bulk values for energies of electron beam for the maximal 10-GeV e-beam energy in the IP. Section 3.d details the choice of the linac settings required for spin transparency.

Polarized electrons with initial energy of 5 MeV are injected into the first ERL with a 500-MeV superconducting linac. They pass twice through this linac before entering the main ERL.

Table 3.a.1 Energy and relativistic parameters of electrons in the low energy ERL: $\Delta\gamma_1 = 965.75$

Pass	E in, MeV	E out, MeV	γ	γ
1	5	498.5	9.78	975.53
2	498.5	1000	975.53	1956.93

Table 3.a.2 Energy and relativistic parameters of electrons in the main ERL: $\Delta\gamma_2 = 4403.10$

Pass	E in, MeV	E out, MeV	γ	γ
1 – linac 1	1000	3250	1956.93	6360.04
2– linac 2	3250	5500	6360.04	10763.14
3– linac 1	5500	7750	10763.14	15166.24
4– linac 2	7750	10000	15166.24	19569.34
eRHIC IP	**10000**		**19569.34**	

The main ERL has two linacs with a nominal energy gain of 2250 MeV per linac. Passing twice through each linac, the e-beam reaches maximum energy of 10 GeV. During the process of acceleration in the ERL, the electron beam passes through the arcs where it loses about 2.5 MeV of its energy in the form of synchrotron radiation.

At full energy, the e-beam passes through a half arc towards the IP. A Compton laser polarimeter installed in the dogleg just before this acquires final measurements of the e-beam's polarization in the IP (note that the dogleg does not affect the polarization, see section 3.d).

Each normal arc or transfer line of the ERL ensures a delay in e-beam time equal to an integer number of RF cycles. In this case, all linacs will synchronously accelerate (or decelerate) electrons. The last arc with the IP and vertical chicane is a special one – it provides for a delay in the e-beam time equal to an integer number plus a half of RF cycles to change the accelerating sequence into a decelerating one. It also incorporates a special cavity to compensate for the synchrotron radiation losses. Section 3.h addresses details of the synchronization, RF cavity phasing and collision frequency adjustment.

The decelerating schedule for the e-beam is just the inverse of that in Tables 3.a.1 and 3.a.2. The electrons pass twice through the same linacs and arcs in the main ERL to decelerate to 1 GeV:

Pass - decelerating	E in, MeV	E out, MeV
1 – linac 1	10000	7750
2– linac 2	7750	5500
3– linac 1	5500	3250
4– linac 2	3250	1000

This sequence matches the e-beam energy in each arc in both accelerating and decelerating processes; hence, there is a significant reduction in the cost of magnetic lattice of the ERL.

Finally, the 1 GeV e-beam decelerates in a low energy ERL to an energy of about 5 MeV and is damped. A damping energy of about 5 MeV insures the absence of residual radiation in the damp, i.e., the damp looks like a "simple" but shielded 2 MW heat source.

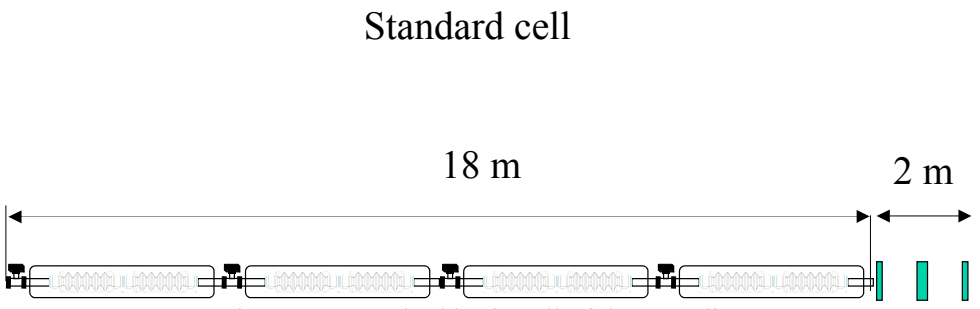

Fig. 3.a.2. Standard basic cell of the ERL linac

Each linacs of the main ERL is comprised of fifteen standard basic cells. Each standard cell (shown in Fig. 3.a.2) contains 4 super-cavity structures and a set of magnetic quadrupoles with constant gradients (leading to and for a linearly growing □-

function [3.a.12]). Each superstructure consists of two 5-cell superconducting accelerating cavities sharing one helium tank and high-efficiency ferrite high-order mode (HOM) - absorbers (the cavity is described below). The use of large aperture RF structure [3.a.1] with effective HOM absorbers is unique to BNL's approach to the ERL. These arrangements assure both a reasonable average accelerating gradient (of about 9-10 MeV/m) and very high stability of the re-circulating e-beam.

The low energy linac, which determines the ultimate stability of the e-beam , has a similar structure but has quadrupoles filling each gap between the helium tanks thereby obtaining lower values of the □-function without significant beating In addition, the first few of low energy accelerating cavities (i.e., those accelerating and decelerating the e-beam between 5-100 MeV) have individual HOM tuners to further increase the e-beam's stability.

Main components of ERL linac

- Five-cell high-current superconducting accelerating cavity
- standard design, normal temperature quadrupoles in linac
- standard design, normal temperature quadrupoles and dipoles in FODO lattice arcs

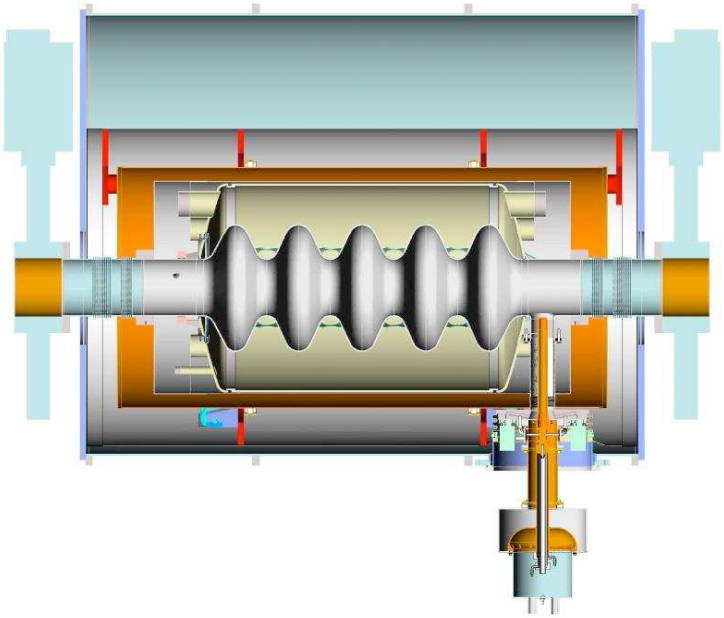

Fig. 3.a.3 A 3-D computer-generated model of the prototype five -cell 703.75 MHz superconducting cavity [3.a.1].

The most important individual component of the ERL is the five-cell superconducting RF (SRF) cavity – a first SRF cavity designed specifically for high-current ERLs [3.a.1]. Its unique features are the key for the proposed eRHIC scheme.

Several factors influenced the choice of key parameters of the cavity.

1. A frequency of 703.75 MHz was chosen due to both physics and engineering issues. This is the 25th harmonic of the RHIC bunch repetition frequency with 360 buckets. A small loss factor from HOMs and the possibility of a larger aperture were important criteria. Also, engineering issues such as the availability of high-power CW klystrons and chemical-cleaning facilities played an important role. A potential future use of this cavity in a linac-ring version of eRHIC (electron-ion collider) also was considered.
2. A five-cell structure with a large aperture of 19 cm was selected in the original design [3.a.2] to optimize the cavity for the best possible damping of higher-order modes. However, further investigation revealed that a 17 cm aperture gave higher acceleration efficiency while effectively damping all HOMs.
3. Ferrite absorbers have proven successful in single-cell cavities (CESR & KEK-B). Following the Cornell design, we adopted them in a five-cell linac cavity.

   The HOM absorbers adequately damp all modes in the cavity that might lead to beam instabilities. Using two ferrite absorbers located along the beam pipe at room temperature simplifies the design. Additional HOM couplers installed in the cavity may prove useful for tuning HOMs in individual cavities to further increase the beam's stability.

The cavity geometry was constructed using "Build Cavity code" "[3.a.4], a graphics interface software to Superfish. It allows the user to specify multi-cell cavity parameters and optimizes the cavity's geometry through a series of Superfish runs. Figure 3.a.4 shows the cavity design with 17 cm aperture and a 24cm beam pipe.

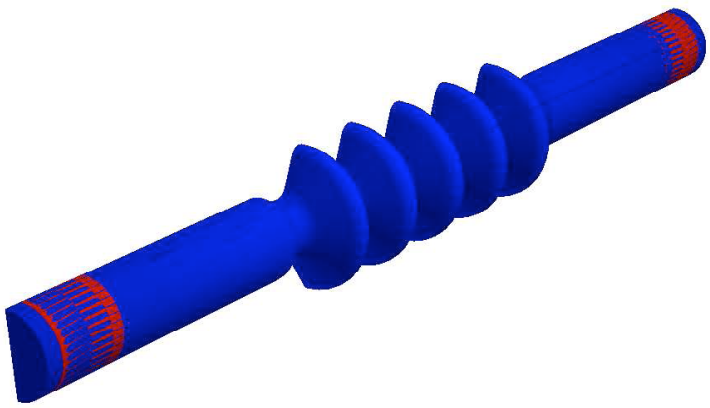

Fig. 3.a.4 Mafia-generated 3D geometry of cavity with enlarged beam pipe and ferrites.

The ferrite absorbers, 24 cm in diameter and 20 cm long, are located outside the cryostat at room temperature. The ferrite material used is Ferrite-50 and is manufactured by ACCEL according to the Cornell design. Various parameters of the five-cell cavity are shown in Table 3.a.3. The optimum iris diameter of 17 cm is compared to an earlier choice of 19 cm.

Table 3.a.3: Cavity Characteristics

Iris Diameter (cm)	17	19
Frequency (MHz)	703.75	703.75
G (Ω)	225	200
R/Q (Ω)	807	710
Q @ 2k	4.5×10^{10}	4×10^{10}
E_p/E_a	1.97	2.10
H_p/E_a (mT/MV/m)	5.78	5.94
cell to cell coupling	3%	4.8%

For the calculation of Q at 2K, we assumed $R_{BCS} = 3n\Omega$ *, and* $R_{residual} = 2\ n\Omega$.

Field flatness and surface fields for the fundamental modes, calculated using 2D FEM code [3.a.5], is similar to the Mafia results shown in Fig. 3.a.5.

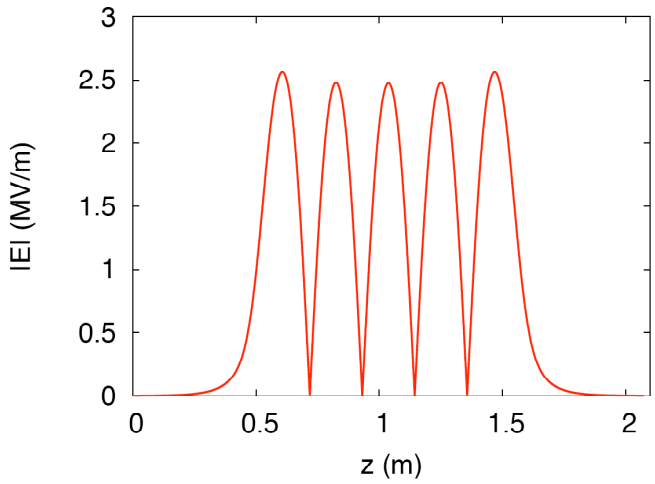

Fig. 3.a.5. Field flatness of the fundamental mode peak-peak 96.5%.

The complex structure of multi-cell cavities often cause modes to be trapped inside the cavity, thus limiting the beam's performance due to instabilities. There are two main reasons for HOMs to become trapped inside the cavity structure:

1. The geometry of the end cell differs from that of the middle cells. This may result in poor cell-to-cell coupling and thereby trap HOMs.

2. Some HOMs may occur below the cutoff frequency of the beam pipe, so preventing the mode from propagating out of the structure. These modes exponentially decay in the beam pipe before they reach the ferrite absorbers.

It is very important to carefully analyze such trapped modes and to modify the cavity structure accordingly to propagate them. It is common practice to use HOM couplers to couple out some harmful modes that exist in these complex structures. A preliminary design for couplers is underway at BNL. However, we propose a cavity design that will demonstrate the possibility of a high current operation with just ferrite absorbers placed in the warm section, thus minimizing cryogenic losses and simplifying critical engineering issues.

The cavity's geometry was optimized for higher-order modes using Mafia's e-module with inverse solver[9]. An initial geometry using a 19cm iris was proven to have three trapped dipole modes (TM1xx) causing the beam to break up at when operating at high current. Analysis of several combinations of cavity iris and beam-pipe radius showed that an iris of 17cm and beam radius of 12cm was an optimized design for both fundamental efficiency and preventing the trapping of harmful dipole modes. The Q values of the dipole modes can directly indicate possible trapped modes. Fig. 3.a.6 shows dipole Qs as a function of frequency for different beam-pipe diameters. A different method exploiting boundary conditions to calculate the coupling of cavity dipole modes to the beam pipe's diameter yield similar conclusions that all modes couple to the beam pipe and will be adequately damped by ferrite absorbers. The factor k shown in Fig. 3.a.6 is a measure of relative field strength between the middle cells and end cell. Fig. 3.a.7 shows a similar calculation for monopole modes.

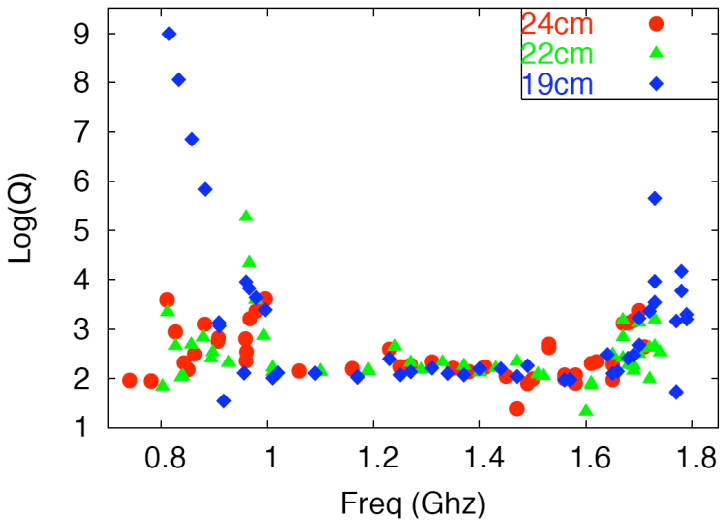

Figure 3.a.6: Dipole Q dependence for 17 cm iris and various biam-pipe diameter geometry.

[9] complex eigenvalue solver

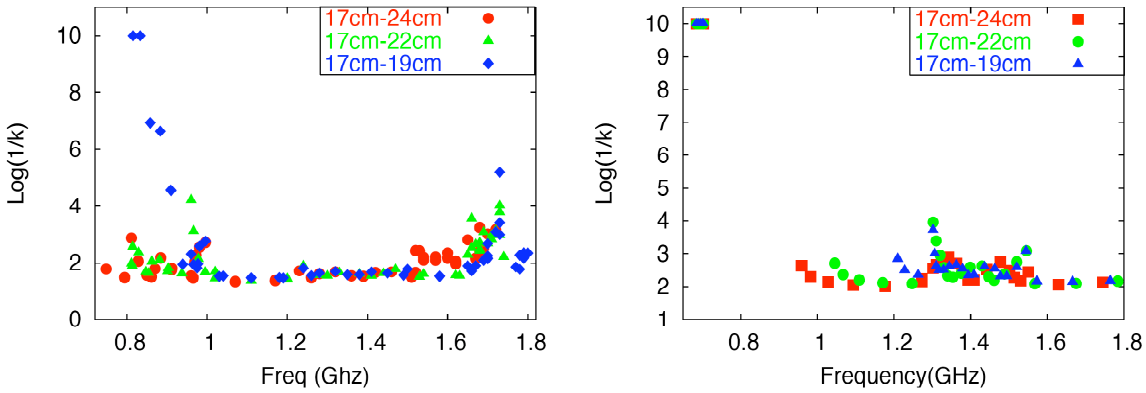

Figure 3.a.7: Analysis of trapped modes in loss-free case. A. Dipole, B. Monopole

The R/Q values for the cavity modes can be easily computed using perturbation methods in MAFIA. It is most desirable to design a cavity with a high fundamental R/Q while keeping the R/Q for dipole modes as low as possible. We find that the R/Q values for dipole modes are quite small for our geometry. Table 3.a.4. shows a few modes with the highest R/Q.

Table 3.a.4 : R/Q and Q Values for Six Dipole Modes of Interest

Frequency (MHz)	R/Q (□)	Q
862.6	30.1592	623.266
882.2	54.6518	2499.858
906.9	41.719	1133.058
967.1	3.5272	3212.957
979.2	3.7425	4608.0
995.7	1.7205	8088.546

The MAFIA results were crosschecked using HFSS [6]. Since HFSS only computes in 3D, the exact input used in MAFIA was replicated in 3D in HFSS and dipole Qs were computed. We were able to extract the dipole Qs of particular modes of interest. Fig. 3.a.8 shows that the MAFIA values agree well with those of HFSS. This is additional proof that our cavity structure is indeed HOM free. Spell out HFSS

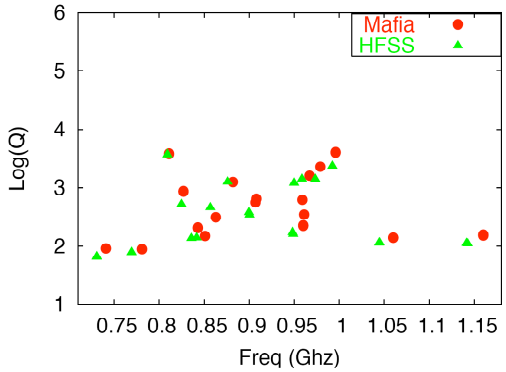

Figure 3.a.8: Dipole Qs from MAFIA and HFSS for the 17 cm geometry

Multi-bunch instabilities are an important issues for any ERL. The energy recovery mode, and high currents contribute strongly to coupled bunch instabilities due to the poorly damped higher modes that limit the cavity's performance. The low frequency dipole modes are particularly dangerous and cause breakup of the beam. We find most dipole Qs to be small with a few of the order of 10^3, but still they do not pose any significant threat. This feature remains to be checked in the high-frequency range (above 2 GHz), but contributions from high-frequency modes to the break up of the beam usually are small. Also, we find that R=Q values are small for all modes which indicate that the threshold currents for such breakup are high. We used the TDBBU simulation code developed in Jefferson Laboratory [3.a.7] to calculate these breakup thresholds from R=Q, Q, and corresponding frequencies, along with other beam parameters as input. We simulated each cavity as two drifts with an energy gain of 13.5 MeV with the HOMs placed inbetween the drifts. Using each dipole mode in both polarizations with a 15 MHz Gaussian distribution, we obtained a threshold current of 1.8 A. Work is underway to accurately build a cavity matrix and optics for the beam to propagate around the ring. In principle, this approach should increase the threshold currents. A sister simulation software called MATBBU [3.a.8] was recently acquired from Jefferson Laboratory that solves an eigenvalue problem to determine the threshold limits; the results give a threshold current of 1.85 A. Fig. 3.a.9 shows the transverse beam's position as a function of time calculated by TDBBU for a current of 1.8 A. The initial (artificial) transverse kick decays, showing that 1.8 A is a stable operational current.

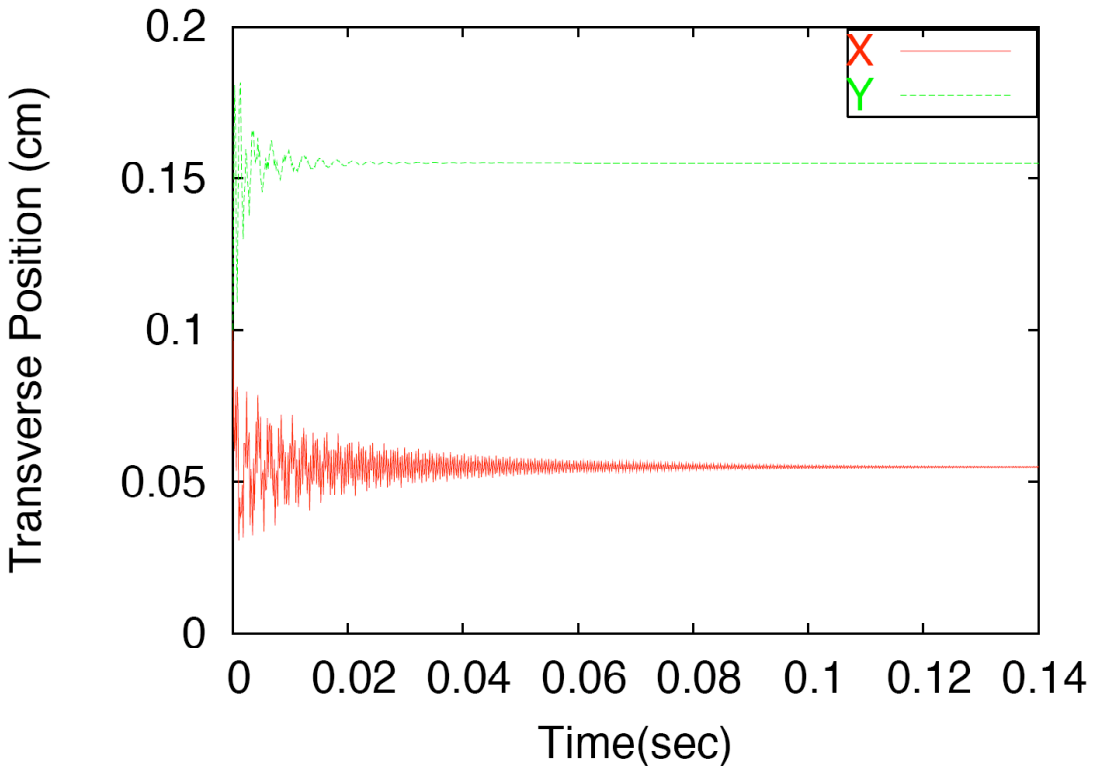

Figure 3.a.9: Simulation of beam breakup in TDBBU with a threshold current of 1.8 A.

One of the major issues in SRF cavity design is power dissipated in the HOMs. High current and high bunch charge implies a huge HOM power that has to be absorbed by the ferrite absorbers or extracted through HOM couplers. When this power is large it becomes a major cryogenic challenge, so it is imperative to keep HOM power loss to a minimum. The HOM power is given by

$$P_{HOM} = f_{beam} k_{loss} q^2$$

where f_{beam} is the beam-repetition frequency at a bunch charge q, and k_{loss} is the loss factor which is given by

$$k_{loss} = \frac{1}{2\pi} \int_0^{\infty} Z_r(\omega) d\omega .$$

In the neighborhood of the resonance frequency, the integral simplifies to the following expression: use normal size type

$$k_{loss} = \frac{\omega_n R_n}{4 Q_n}$$

where loss factor was calculated with ABCI, using a single bunch with a 1cm RMS length. The loss factor results are displayed below in Fig. 3.a.10.

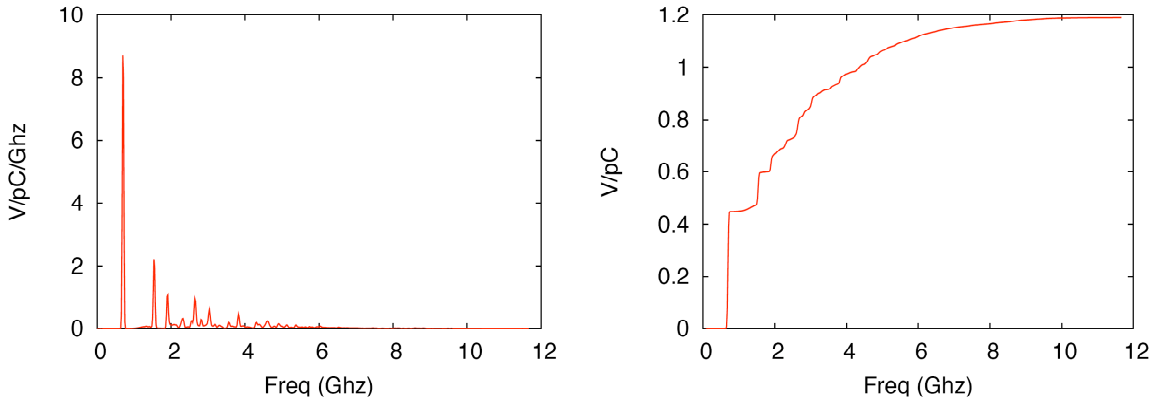

Figure 3.a.10: Loss Factor and integrated loss factor for 17-24cm geometry

Another important factor to consider is wall losses due to the fundamental mode in the beam pipe. Since part of the beam pipe is at 2K, it becomes crucial to minimize this loss so that CW operation becomes feasible. Preliminary calculations from BNL's cryogenic group [3.a.13] indicate a maximum loss of 25 watts will be tolerable for a sustained CW operation. This power loss can be calculated with MAFIA. Thus, for a beam pipe 20-cm long made of copper after the end cell with our present configuration shows a total wall loss less than 10 watts on both sides of the cavity. We expect to intercept this power at liquid nitrogen temperature. The copper tube, also serving as a shielding for the stainless-steel bellows, will be anchored to the radiation shield and thermally isolated from the niobium pipe. The electrical path for HOM power and beam image currents will be

provided by a small capacitive element.

Simulations for a low energy prototype of the ERL showed that *threshold current for the transverse beam breakup is as high as 1.85 A for a single pass (i.e., ~ 0.9 A for two passes)*. The main reason for this very impressive result is strong damping of the HOM in the advanced five-cell cavity design described above with large sized irises and ferrite absorbers.

The PERL design studies [3.a.11] demonstrated that choosing a focusing optics in the linacs with β-function proportional to the e-beam energy sets conditions for improved beam stability, assuming that arcs properly match β-function and the phase advance is proper. The above conditions allow element M_{12} to come very close to zero for all individual cavities.[10]

Presently, detailed designs are underway for

- Lattice for the linacs
- Lattice for the arcs
- Longitudinal dynamics in the ERL
    - Including Polarization effects (see also section 3.d)
- Losses for synchrotron radiation
- Energy recovery and beam dump

Layout and Optics of the linac – on of the options for ERL [3.a.14]

The linac recirculates the beams to reduce the number of cavities needed to reach the final beam energy. A recirculating energy-recovery linac consists of three distinct building blocks:

- The linacs that accelerate and decelerate the beam. Beams of different energies can be in the linac simultaneously.
- The arcs that bend the beams around to reinject them into the linacs. A separate arc must be used for each beam energy.
- The spreader/recombiner sections that distribute bunches from the linac into the arcs according to their energy.

Since the number of arc beam lines increases proportionally to the number of passes through the linacs, and the current threshold for multibunch instability decreases with the number of passes, only two passes are used in the eRHIC.

The focusing in the linacs is determined by the lowest beam energy. Overfocussing must be avoided. For that reason, a two-stage scheme is used (Fig. 3.a.11). The beam is generated by an RF gun and accelerated to about 10 MeV. It is injected into the first-stage linac with 12 cryo modules and accelerated to 1.018 GeV using one recirculation. The second stage uses a racetrack layout, similar to the CEBAF accelerator, that minimizes the tunnel's length.

[10] Detailed studies of theoretical aspects of ERL beam dynamics also are in progress

The two linacs are parallel. Accordingly, the linacs can be lengthened in future upgrades with a minimum amount of concrete work. A triangular layout also could be adopted , that would lower synchrotron-radiation power, but at the cost of a longer tunnel.

Each of the two linacs has 60 cryo modules for an energy gain of 2.268 GeV per pass. The beams are focused by quadrupoles in a F0D0 arrangement. In contrast to the CEBAF accelerator where the field gradient increases with the beam's energy, the quadrupole field is fixed. In such a lattice, the beta functions oscillate around an average value, which increases with the beam's energy. Since the linacs are optically symmetric, a mismatch and large beta beat is avoided. Small beta functions increase the threshold for the multi-bunch beam breakup. Fig. 3.a.12 shows the beta functions for all passes of the second-stage linac.

The arc length is given by the allowed synchrotron radiation power that must not exceed 7 kW/m in the highest energy arc. This requires a bending radius of 155 m in the arc dipoles. The arcs must be isochronous so that the initial energy spread of the beam does not cause bunch lengthening in the first arc which would increase the energy spread in the next linac, and so on. The arc dipoles are 5 meters long with a field of 2 kG at 10 GeV. The arc cell, consisting of twelve dipoles (Fig. 3.a.13), has a fill factor of 68% (integrated dipole length over total length). The average radius of the arc is 250 m. The dispersion function is zero at both ends of the cell, thereby allowing the insertion of the interaction region in the 10 GeV arc and of dogleg dipole magnets for variation in path length in the lower energy arcs.

The spreaders/recombiners separate the beams horizontally. Since there are only two beam lines in the arc tunnels this does not make the magnets inaccessible as it would in the CEBAF with five beam lines. Further, there is no need to match the vertical dispersion. The horizontal dispersion can easily be matched by modifying the quadrupole strength in the first arc cell. Figs. 4 and 5 show the spreader for the north end and the south end of the linacs, respectively.

To protect the superconducting cavities from the synchrotron radiation, the first dipole of the spreader has a low field of 200 Gauss, resulting in a bending radius of 1500 m at 10 GeV. The total radiated power from this dipole is 70 Watts. Half of this power can be removed with a collimator in front of the first cryomodule. Since the inner diameter of the cavities is 17 cm, the remaining radiation will go through the cavities without hitting the walls. A second collimator (and maybe third) inside the linac will remove this radiation.

The optics of the interaction region optics are similar to those used for the ring-ring version (Fig. 6). However, since the beta function in the interaction point is much larger (92 cm), the beta function in the focusing quadrupoles is much smaller. Figure 7 shows the fan of synchrotron radiation created in the interaction region; it must not hit the beam pipe inside the interaction region. Fig. 7 shows that the IR must be antisymmetric to accomplish this. A detailed layout of the arcs and interaction region is being developed.

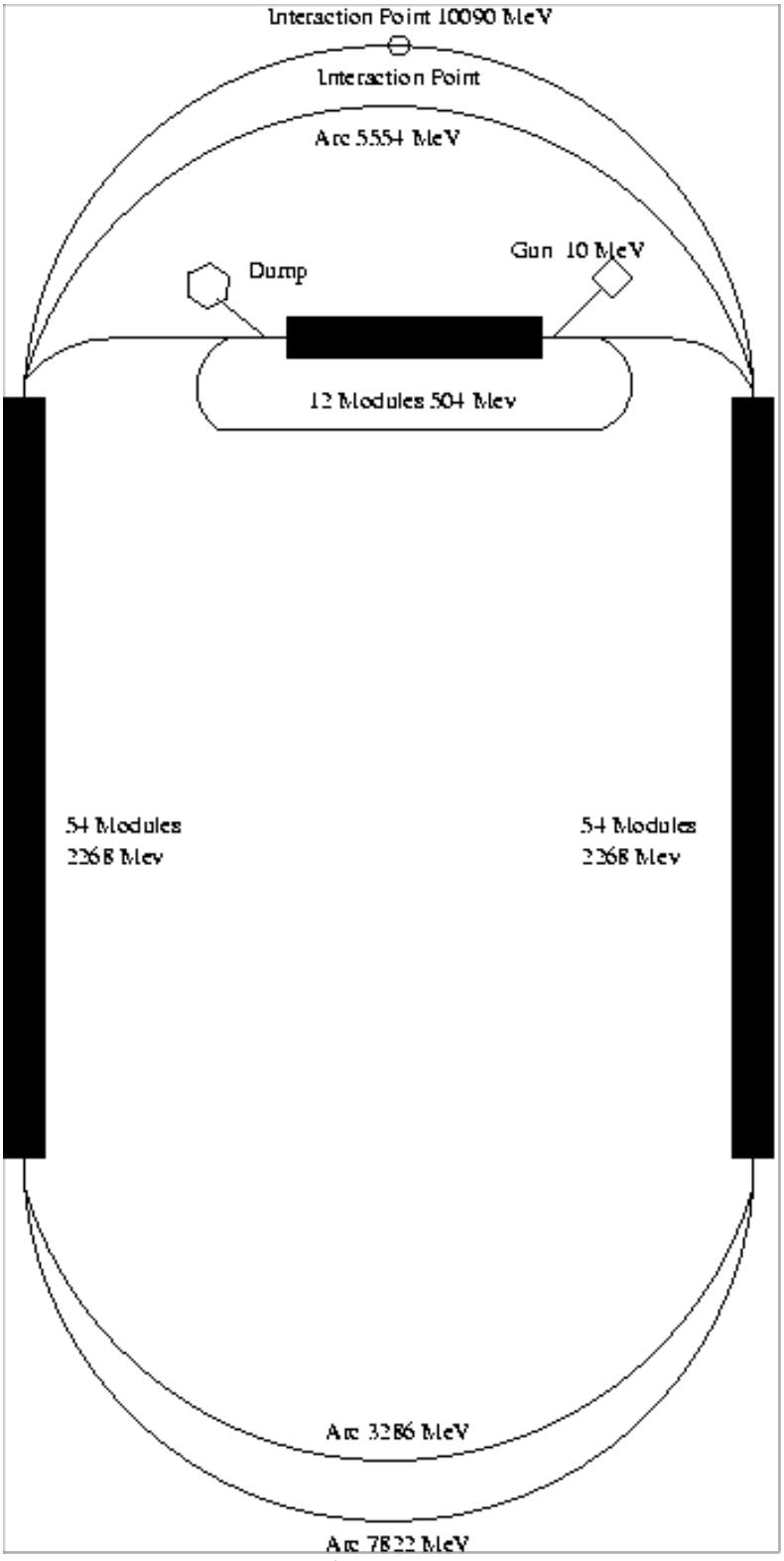
Interaction Point 10090 MeV
Interaction Point
Arc 5554 MeV
Gun 10 MeV
Dump
12 Modules 504 Mev
54 Modules
2268 Mev
54 Modules
2268 Mev
Arc 3286 MeV
Arc 7822 MeV
Figure 3.a.11

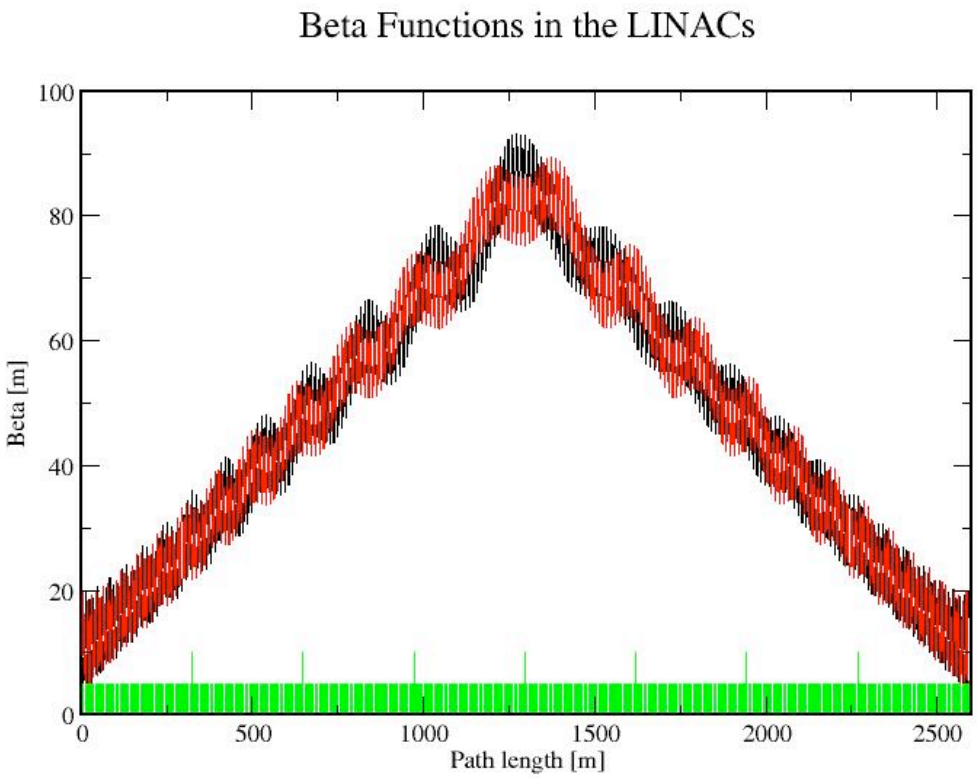

Figure 3.a.12 Beta functions (black horizontal, red vertical) of all Linac passes. The arcs are represented as thin matrix elements, shown as tall green lines.

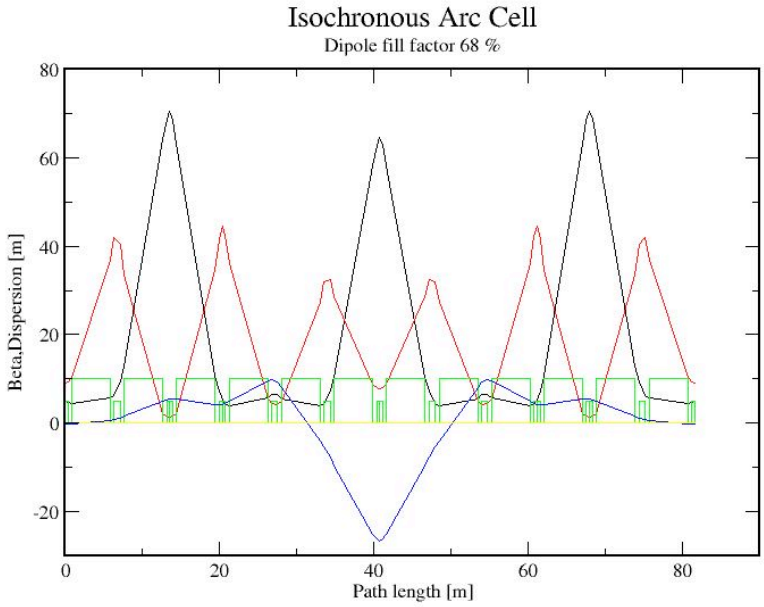

Figure 3.a.13. Arc cell

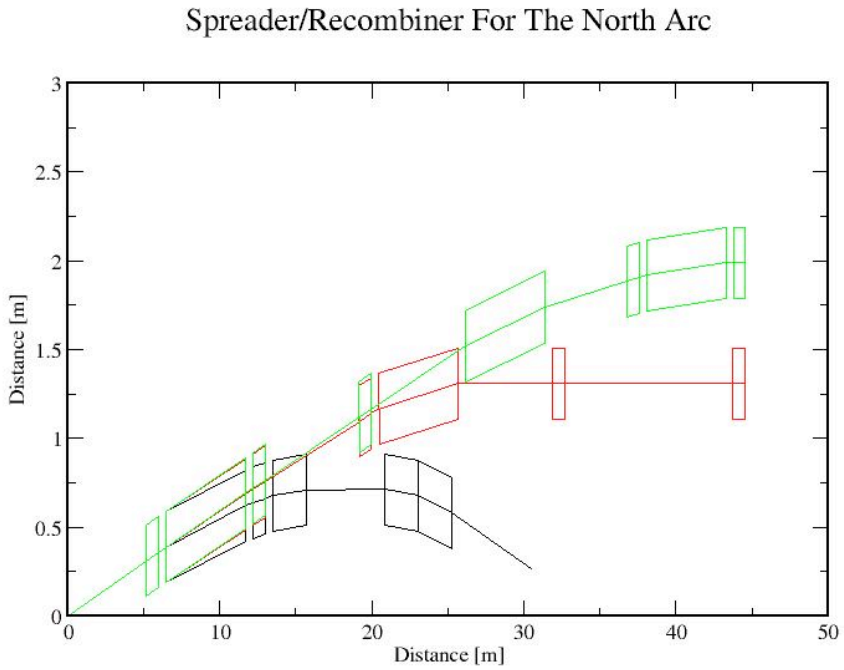

Fig. 3.a.14: Beam spreader/recombiner for the north end of the linac for the injection/extraction line (black), the 5.5 GeV line (red), and the 10 GeV line (green).

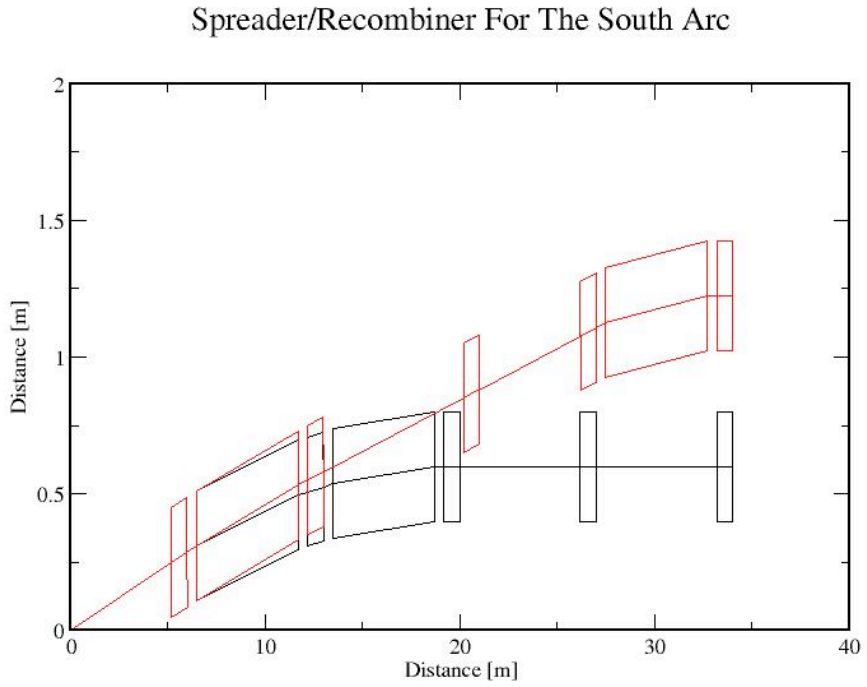

Fig. 3.a.15: Beam spreader/recombiner for the south end of the linac for the 2.25 GeV line (black) and the 7.75 GeV line (red).

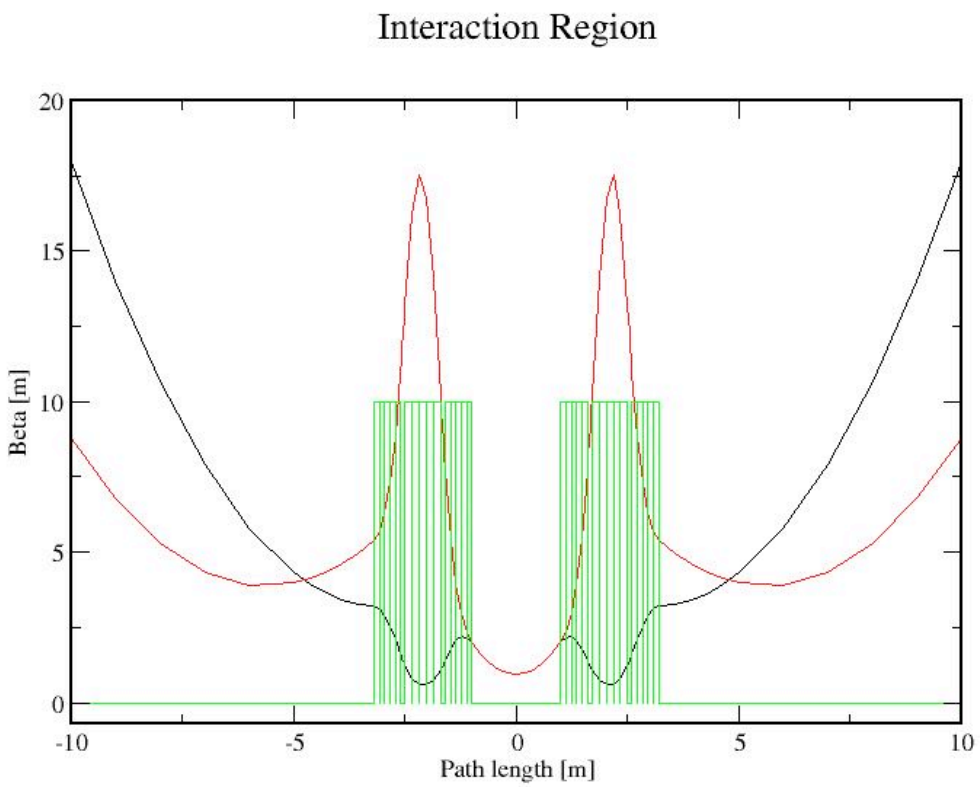

Fig. 3.a.16: Interaction region optics

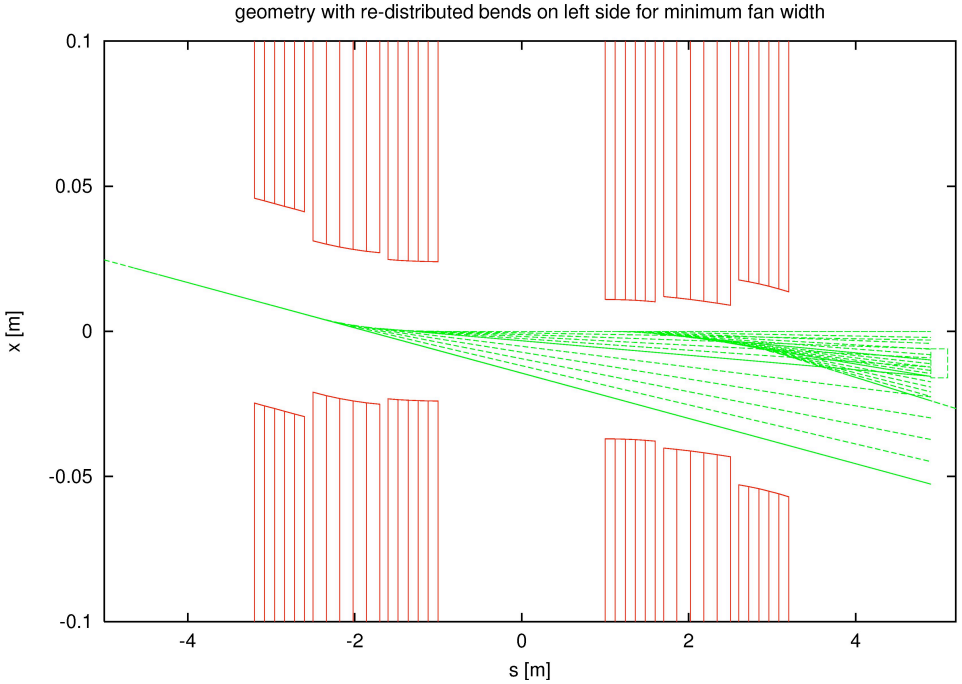

Fig. 3.a.17: Radiation fan in the interaction region. The radiation created in the interaction region must be absorbed outside the beam pipe.

References

[3.a.1] R. Calaga et. al., Proceedings of SRF2003, Travemünde/Luubeck, September 2003.
[3.a.2] Dong Wang et. al., PAC 2003, Portland, May 2003.
[3.a.3] The MAFIA Collaboration, MAFIA Version 4.0, CST, GmbH, Darmstadt, Germany.
[3.a.4] Paolo Pierini, Build Cavity Manual, Milan, Italy.
[3.a.5] J. Sekutowicz, Proceedings of Linear Accelerators Conference, Tsukuba, Japan, 1994.
[3.a.6] High Frequency Structure Simulation (HFSS), ANSOFT Co., Pittsburgh, PA, USA.
[3.a.7] TDBBU was written by G.A. Krafft at Jefferson Laboratory.
[3.a.8] MATBBU was written by G.A. Kraft at Jefferson Laboratory.
[3.a.9] Advanced Energy Systems, USA.
[3.a.10] E. Chojnacki et. al., Proceedings of the Particle Accelerator Conference, 1997
[3.a.11] V.Yakimenko et al., PERL design paper
[3.a.12] V.Litvinenko, eCooling group, Internal Note, August 2003
[3.a.13] Mike Iarocci, Private Communication
[3.a.14] Jörg Kewisch, Vladimir Litvinenko, Christoph Montag, Daniel Anderson, C-AD, Working material, BNL, January 14, 2004

3.b Polarized electron gun

The following description highlights the common part with a description of the main requirements and parameters of the polarized gun in the main section of the ZDR (Sec. 2.3.1, Polarized Electron Photoinjector by M. Farkhondeh and W. Franklin), as well as focusing on issues specific for the ERL-based eRHIC.

Introduction: The advancement in the polarized electron source technology over the past decade at nuclear and particle physics accelerator centers have been substantial [3.b.1-3]. Highly polarized electron beams of diverse peak currents, time structures and duty cycles including CW beams are now routinely produced at Jefferson Lab, SLAC, HERA, MIT-Bates, Mainz and Bon [3.b.1-5]. These polarized injectors are based on photoemission process from strained GaAs based photocathodes illuminated by laser radiations at 800-850 nm followed by an extraction process with high gradient electric field. At MIT-Bates, long pulses with 2 mA currents of highly polarized electron are now routinely achieved.

High polarization photocathodes: Polarized electron beams for accelerators are generated by photoemission process using longitudinally polarized laser lights at 750-850 nm from the surface of GaAs based photocathodes under UHV conditions. The electrons are extracted from the surface using high gradient field present between the anode and cathode electrodes. The maximum theoretical limit for degree of polarization from a bulk GaAs surface is 50% and ~40% in practice due to depolarization effects in the bulk. The photoemission process in bulk GaAs is the simultaneous excitation of electrons in degenerate states in the valance band to the conduction band. To the degree that this degeneracy in the valance band is removed, higher degree of polarization can be achieved. A common technique to remove the existing degeneracy is to introduce strain in the lattice by growing GaAsP layers on substrate GaAs. The lattice mismatch between GaAs and GaAsP produces mechanical strain near the boundary surface [3.b.6]. The active layer must be very thin of the order few hundred nm to keep the strain present near the surface of the photocathode. The reduced depth in the active layer causes a substantial reduction in the Quantum Efficiency (QE) of the photocathode. QE is the fractional number of electrons generated by a single photon. QE for bulk GaAs photocathodes with pol~30-40% is of the order of 1-10 % and 0.01-0.1% for high polarization strained GaAsP, smaller by two decades. The high polarization photocathodes therefore, have the inherent problem of low QE's. With a laser radiation of wavelength λ and power P, the maximum peak current generated from a photocathode of appropriate band gap structure is given by

$$I(mA) = \frac{QE \times P(mW)\lambda(nm)}{1239}$$

For instance, with P=1kW, QE=0.1% at λ=800 nm, a current of ~0.64 A can be generated. As shown in Figure 3.b.1, the QE and polarization are strong functions of λ.

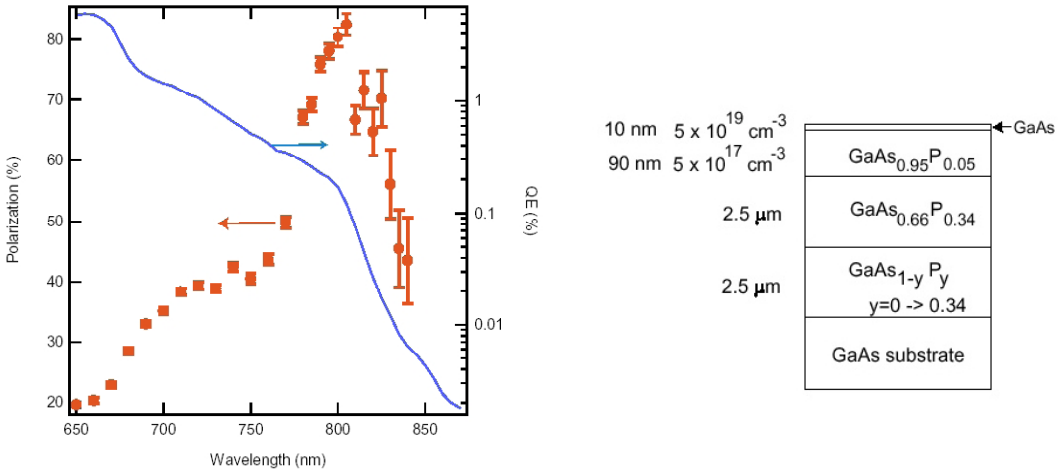

Figure 3.b.1. (Left) Photoemission data on a GaAsP from SLAC [3.b.7] showing Polarization and QE as a function of wavelength. (Right) A schematic diagram of the lattice structure of a high polarization high gradient doped strained GaAsP photocathode [3.b.8] now in use at SLAC and MIT-Bates. The peak polarization for this sample is near 800 nm where commercial high power lasers are more readily available The 10 nm thick layer is highly doped to reduce the surface charge limit effect.

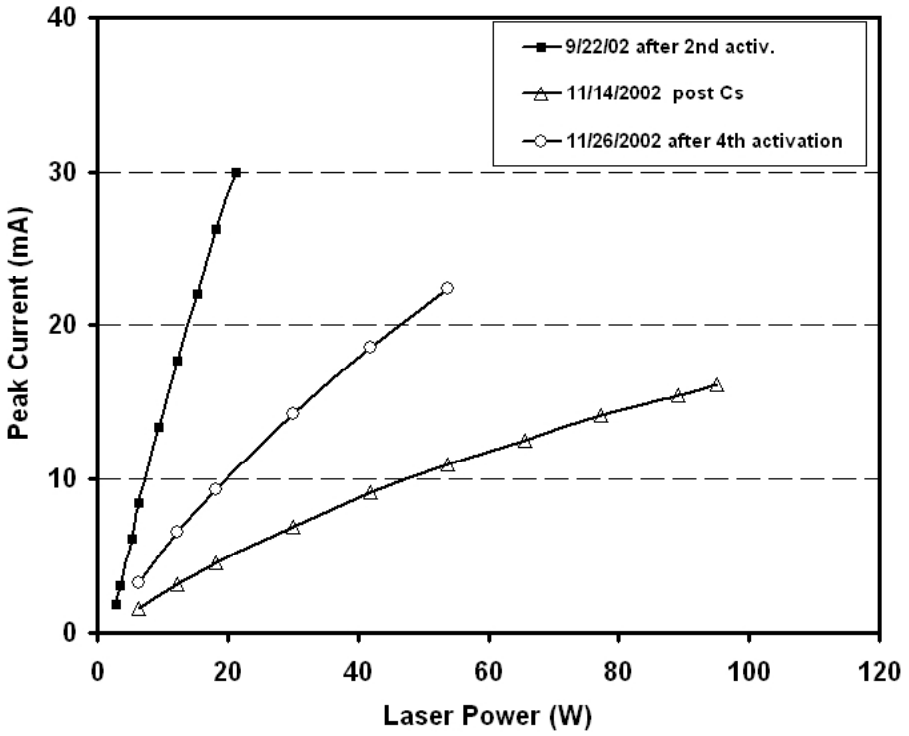

Figure 3.b.2. Peak current vs. laser power shown after several heat cleaning and activations for a two months period for the MIT-bates polarized injector. Due to surface charge limit effect the slope of the current vs. laser power decreased between 9/22 and 11/26 (squares and triangles). A heat cleaning and activation on 11/26 partially restored the slope (circles).

Surface Charge Saturation effect: In a perfectly atomically clean and freshly activated photocathode, the extracted charge is proportional to the incident laser power. However, as the QE of the photocathode decreases due to surface pollution, the relationship between the laser power and the extracted charge begins to deviate from linear. This is particularly pronounced at high laser power densities where due to an abundance of negative charges on the surface, the effective work function near the surface is increased causing a reduction in the extracted charge per bunch. This effect has been observed at SLAC and at MIT-Bates and studied in great detail at SLAC [3.b.8]. Figure 3.b.2 shows data from the MIT-Bates polarized injector that clearly indicates the deviation from linear as the photocathode is aged over the course of many months. As charge saturation effect increases more laser power is required for producing the current required. To reduce the surface charge limit in the high gradient doped sample currently used at SLAC and MIT-Bates, the top 10 nm GaAs layer is heavily doped. However, this thin layer is evaporated after several heat cleaning at near 600 C. Cares must be taken to reduce the number of heat cleaning for as long as possible. There are potentially several other methods to reduce the surface charge limit for high polarization photocathodes. These include cathode biasing, higher gun voltage, higher QE and the use of superlattice structures [3.b.9]. These methods have been tested in various photocathode and gun R&D programs mainly at SLAC and Nagoya but further R&D is required to make them practical.

Issues specific to linac-ring based eRHIC: The 0.5 A average current of highly polarized beam from a polarized electron source for injection into an ERL linac is a demanding task and has not yet been accomplished. At 28.1 MHz eRHIC collider frequency and bunch lengths of 100 ps, bunch charges of 18 nC are needed from the polarized source. Usage of longer bunch combined with bunch compression should help to ease the current requirements. Using a simple linear scaling extrapolation of results achieved at J-Lab and elsewhere, it may be possible to produce such high average currents assuming that sufficient laser power is available. For instance, the polarize source at J-Lab with a laser spot size of ~ 0.2 mm diameter, routinely produces ~100 μA current at 500 MHz and is beginning to produce ~40 μA for the G0 experiment at ~30 MHz [3.b.1]. With the same laser power density as J-Lab, to produce 0.5 A at 30 MHz, a laser spot size and illuminated photocathode area of 14 mm in diameter is needed. In this case, the required laser power for a high polarization GaAs based photocathode with QE of ~5×10^{-4} would be in the kW range, a level that may only be produced with a future ERL-based free electron laser linac as discussed later in this section. It may also be possible to reach this high level of laser power using an array of high power diode array laser systems used for the MIT-Bates polarized injector. It should however be emphasized that this is a simple scaling extrapolation and the required current of 0.5 A is about three orders of magnitude over the current produced with a CW linac today. It should also be noted that to date unpolarized currents as high as 5-10 mA have been produced from a 3-5 mm laser spot on a bulk GaAs photocathode at the J-Lab's ERL-FEL [3.b.11].

An important issue that requires R&D is the surface charge limit effect described [3.b.7] in detail in the eRHIC ZDR section 2.4. This phenomenon can often place a severe limit on the maximum amount of charge that can be extracted from the photocathode regardless of the level of laser power. Charge limit effects often appear when the QE of the photocathode becomes very small and the surface condition of the photocathode

deteriorates. The beam emittance from a large area photocathode needs to be studied with computer simulation to ensure that it can be brought under control before injection to the linac. A detailed computer simulation with software packages like PARMELA needs to be made of this polarized injector to ensure that proper optics solution can be obtained. Also high average and high peak current photoemission tests need to be carried out in the next few years to ensure that the simple scaling law discussed above is valid. The MIT-Bates polarized injector group has the expertise and a test stand that can carry R&D in high peak and high average current photoemission tests. The test stand at MIT-Bates includes an electron gun, laser systems, beam transport system and a Mott polarimeter that can be used for these R&D efforts if proper level of funding is available.

Another critical issue for a high average current polarized electron source is the lifetime of the photocathode. It is very difficult to study and estimate the lifetime without building an actual gun and beam line. The lifetime of a photocathode is defined as the total time a desired level of electron current can be maintained before the surface of the photocathode needs a heat cleaning and activation. Any additional laser power would prolong this period unless severe charge limit effect is present. At these very high average currents there is no experimental data on lifetime issues of photoemission guns. At high average currents, the lifetime of photocathode is severely shortened by desorption caused by any slight beam loss near the gun chamber. Therefore it is extremely critical that beam optics in the gun chamber and its vicinity are designed very carefully and relative beam losses are $1x10^{-5}$ or better. Beam losses can be further reduced by keeping the laser light clear of the periphery of the photocathode to prevent electrons with extreme trajectories. It is prudent to have a photocathode diameter of at least a factor of two larger than the diameter of the laser spot.

In addition, the heat generated by a kW laser power must be removed from the photocathode assembly that is under UHV condition. Any increase of the photocathode surface would seriously reduce the quantum efficiency by an increase in the rate at which the surface Cs is evaporated at elevated temperatures. The design of the photocathode assembly and the gun should accommodate this heat load.

Requirements for the laser driver for the gun: The latter are defined by the electron beam's parameters, as well as by the photocathode used for generating polarized electrons [3.b.12]. The degree of polarization is the most important parameter for the eRHIC and hence, the wavelength should be chosen at which polarization is maximum, i.e., λ=815 nm where polarization reaches 82% for a strained GaAs photocathodes (see Fig. 3.b.1), or even 90% for super-lattice photocathodes. A high degree of polarization occurs at the wavelengths where the quantum efficiency of the photocathode is rather low, ~ 10^{-3}, hence, the power requirements for the laser-driver are high.

The eRHIC requirements (the maximum electron beam current of 0.45 A) combined with feasible parameters of AsGa strained photo-cathodes give following requirements for the laser source:

○ Wavelength [nm]	815 ± 5	
○ Photon energy [eV]	1.52	
○ Polarization	circular (left/right)	
○ Laser power [W]	475	for 0.15% QE
	2,283	for 0.03% QE
○ Mode of operation	CW	
○ Rep-rate	28.15 MHz	
○ Energy per pulse [□J]	17 - 844	
○ -□Pulse duration [psec]	100 - 200	
○ Peak power [kW]	170 – 8,440	
○ Stability		
▪ Pulse-to-pulse	< 0.1%	
▪ Long term	< 1%	

References:

3.b.1. "*Status of the Jefferson Lab Polarized beam*", J. Grames, AIP proceeding of SPIN2002 Vol. 675 p1047.

3.b.2. "*The SLAC Polarized Electron Source"*, J. E. Clendenin, AIP proceeding of SPIN2002 Vol. 675 p.1042

3.b.3. *"MIT-Bates Polarized Source*", M. Farkhondeh, PESP2002 workshop, Danvers, MA, AIP proceeding of SPIN2002 Vol. 675 p.1098.

3.b.4. "*Status of the polarized source at MAMI"*, K. Aulenbacher, AIP proceeding of SPIN2002 Vol. 675 p1088.

3.b.5. "*The polarized Electron Source at ELSA*", W. v. Drachenfels, AIP proceeding of SPIN2002 Vol. 675 p1053.

3.b.6. T. Maruyama, et. al., Phys. Rev. Lett. **66** (1991) 2376.

3.b.7. T. Maruyama et. al., NIM A492, 199(2002)

3.b.8. Bandwidth Semiconductor Inc., Bedford, NH.

3.b.9. "Suppression *of the Surface Charge Limit in Strained GaAs Photocathodes*", T. Maruyama, AIP proceeding of SPIN2002 Vol. 675 p1083.

3.b.10. Spectra-Physics Opto Power diode laser model OPC-DO60-mmm-FC. Also" *High power Diode Laser System for SHR*", E. Tsentalovich, AIP proceeding of SPIN2002 Vol. 675 p1019.

3.b.11 B. C. Yun, et al., Proc.1999 IEEE Particle Accelerator Conference (1999PAC), P2453.

3.b.12 P. Hartman et al., "Polarized Electron Linac Sources", In Proc. Of The 2nd eRHIC workshop, Yale, CN, April 6-8, 2000, p.120
T. Zwart et al., "Polarized Electron at Bates: Source to Storage Ring", Proc. Of Second EPIC Workshop, Cambridge, MA, 14-15 September 2000, p.343

3.c Laser source for the polarized gun

The requirements of the laser source for the polarized electron gun naturally match those of a FEL driven by a small energy-recovery linac (ERL). The ERL for the FEL should be based on exactly the same technology as the main 10 GeV ERL (but with dramatically lower energy and with much smaller scale). First, the FEL wavelength is continuously tunable and can be chosen to maximize polarization of the e-beam. Second, the time structure and repetition rate of the FEL laser beam, 28.15 MHz, coincides with that of the e-beam, which is the 25th sub-harmonic of the ERL's RF frequency. Third, a FEL based on a helical wiggler generates 100% circular polarization in a single-mode laser beam. Fourth, the power requirements of 0.5 kW to 2.5 kW range match with modern ERL-based FELs [3.c.1]

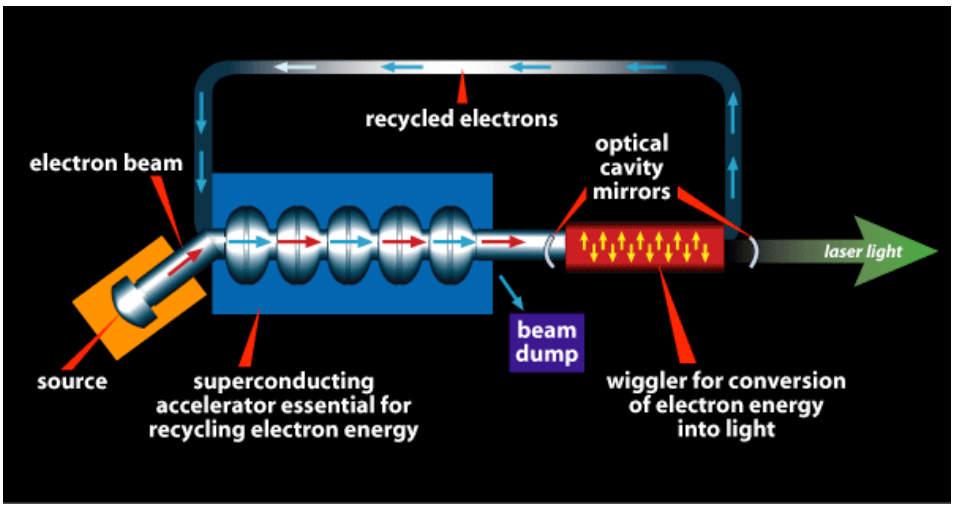

Fig. 3.c.1 Scheme of an ERL-based FEL

Table 3.c.1 gives examples of parameters for the state-of-the-art ERL FEL.

Table 3.c.1. System Parameters of the JLab FELs [3.c.2]

	Achieved	IR 2003
Energy (MeV)	20-48	80-210
Beam current (mA)	5	10
Beam Power (kW)	**240**	**2000**
FEL ext. efficiency	**>0.75%**	**1%**
FEL power (kW)	**2.1**	**>10**
Charge/bunch (pC)	135	135
Rep. Rate (MHz)	18.75-75	4.7-75
Bunch Length* (psec)	0.4 (60 pC)	0.2

The FEL parameters chosen for the eRHIC's polarized gun (see below) are relatively conservative, keeping them well within or very close to demonstrated technology. The relatively high energy of the electron beam allows for both a lower value of the electron beam's current and its better quality. This factor simplifies the propagation of the beam in the FEL and in the ERL.

Table 3.c.2. Parameters of FEL for eRHIC's polarized gun

Electron beam	
Energy [MeV]	**160**
Beam current (mA)	**5**
Beam Power (kW)	800
FEL ext. efficiency	up to 0.75%
FEL power (kW)	**up to 6, nominal - 2**
Charge/bunch (pC)	180
Rep. Rate (MHz)	28.15
Wiggler	
Type	helical with switchable helicity
Length [m]	2 x 0.9
Period, λ_w [cm]	6
Aperture [cm]	1
Wiggler parameter, K_w	1.29 - nominal (tunable within 0-1.5)
Peak magnetic field [T]	0.230 (tunable within 0-0.265)
Laser light	
Wavelength, λ [nm]	815, nominal, (tunable within 400 – 1000 nm)
Chirp [nm/psec]	5
Polarization	100% circular (left/right)
Spot-size in FEL[cm^2]	0.0020
that the mirror [cm^2]	2.08
τ-Pulse duration [psec]	5 (chirped)
Optical cavity	
Length [m]	31.8926
Radius of curvature [m]	15.962
Rayleigh range [m]	0.5
Out-coupling	10%
Intracavity power [kW]	60
CW Power density [kW/cm^2]	30 at the mirror
Peak Power density [MW/cm^2]	205 at the mirror
Laser pulse stretcher	
Input pulse duration [psec]	5, chirp 5 nm/psec
Wavelength [nm]	*815*
Chrip [nm/psec]	*5*
Dispersion section [psec/nm]	20 –40
Input pulse duration [psec]	100 -200

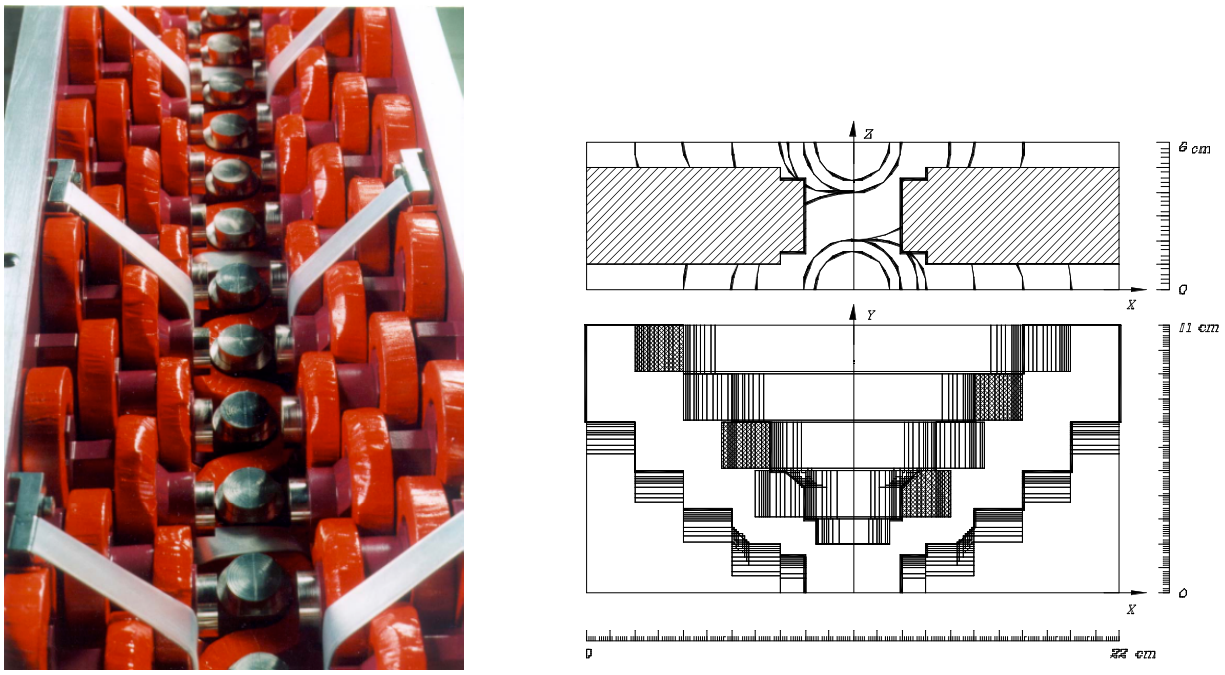

Fig. 3.c.2 Electromagnetic pseudo-helical wiggler with switchable helicity [3.c.3]: On the left, a photograph with the top quarter of the wiggler removed. On the right, there is a drawing of its half-period.

Even though most of these FEL parameters are typical for modern high power FELs, some special features are specifically required for a polarized gun with a low-emittance electron beam:

- Switchable helicity of the FEL photons;
- Wide range of the power control to compensate for degradation of the photo-cathode's quantum efficiency and to extend the time between cathode changes;
- About 2x excess of optical power for giving the laser beam a flat top profile at the surface of the photocathode to maintain low emittance of the e-beam;
- Feed-back on both the FEL power and time-profile of optical pulses;
- Matching the FEL pulse's duration ~ 5 psec with the pulse duration at the gun ~ 100 psec requires a laser pulse stretcher and, therefore, a wavelength chirp in the FEL pulse.

The polarization of the FEL wigglers determines that of the FEL photons [11] – i.e., a planar wiggler imprints linear polarization into the FEL photons, while a helical wiggler imprints circular polarization into them. The need to switch the helicity of circular polarization requires this feature to be incorporated into helical wiggler of the FEL. One possibility of doing so is to use a pseudo-helical electromagnetic wiggler as that shown in Fig. 3.c.2. In this case, the magnetic field is generated by a horizontal- and a vertical-

[11] Assuming that the mirrors of the optical cavity are optically inactive, i.e., do not rotate the polarization.

array of poles with independent controlled strengths via their coil's currents. Horizontal poles are shifted for a quarter of the period with respect to the vertical ones. When both currents are equal, the field has helical structure with *cos*-like dependence of vertical magnetic field and *sin*-like dependence of horizontal one, i.e., the electron's trajectory in this wiggler is helical. The helicity sign can be easily flipped by the changing the sign of the current in one of the coils (for example, the horizontal one). This excellent approach guarantees 100% helical polarization of FEL photons [3.c.4].

The other possibility is to use permanent magnet wigglers, in which horizontal array of magnets can be moved with respect to the vertical [3.c.5]. These wigglers perform reasonably well, but the sign of helicity is switched by slow mechanical movements, and cannot be performed as rapidly and reliably as with an electromagnetic wiggler.

The other required feature is a smooth and wide-ranging control of the FEL power. A scheme of an optical klystron (OK, [3.c.5]) for the FEL can provide this feature. Employing a buncher in the scheme of the optical klystron ensures smooth control of the power limitation by a simple control of the current in the buncher's coil. This feature will be used for maintaining constant electron-beam current when the quantum efficiency drops, as well as for stabilizing the FEL power.

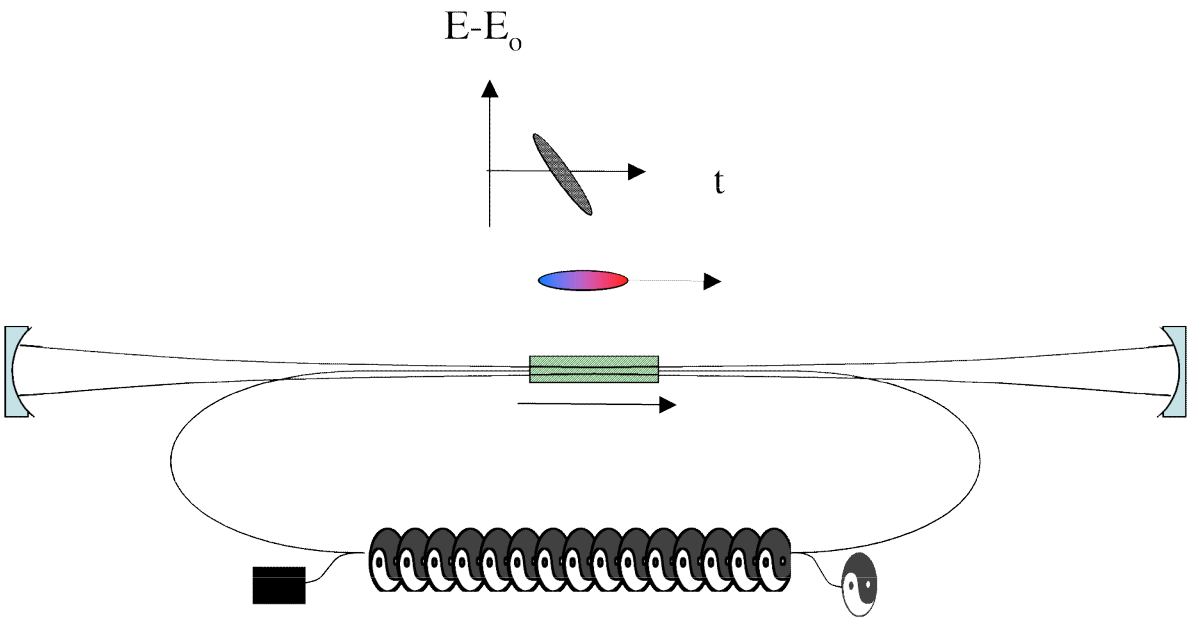

Fig. 3.c.2 Scheme of 6 kW CW FEL for eRHIC polarized gun. The electron beam, injected into the ERL at energy of 6 MeV, accelerated to 160 MeV with an energy chirp of 1.5% per 5 psec, is used in the FEL (where it loses ~ 1 MeV of energy), then decelerated to 5 MeV and damped. *Damping the electron beam at energies below 10 MeV is environmentally preferable because it does not create residual radioactivity.*

The driving electron beam determines the time structure of the laser pulses in the FEL. FEL-gain requirements lead to a high peak current resulting in a rather short laser micropulses (~ 5 psec). Following a well-known FEL technique, we will extend laser

pulses to the required 100-200 ps using wavelength chirp in FEL and the laser pulse stretcher. The wavelength of the FEL photons, defined by well-known FEL formula for a helical wiggler with wiggler period λ_w

$$\lambda = \frac{\lambda_w}{2\gamma^2}\left(1 + K_w^2\right) \qquad (3.c.1)$$

can be controlled either by changing the electron beam's energy or by thewiggler's parameters

$$K_w = \frac{eB_w\lambda_w}{2\pi mc^2}.$$

In our case, we will use both dependencies: K_w will be used to tune FEL to the optimal wavelength, and the dependence of the resonant FEL wavelength on the energy of electrons $E = \gamma mc^2$ will be used to chirp the energy of FEL photons (see Fig.3.c.2 below). By accelerating electrons slightly off-phase, we will imprint the energy chirp into the electron beam. In response to this chirp, the wavelength of the photons has the chirp from the head to the tail of the FEL pulse. Using a dispersive system (i.e., a system with an index of refraction and time of pass depending on the wavelength, which is schematically out-lined below) we will extend the chirped pulse from 5 psec to the desirable duration of 100-200 psec.

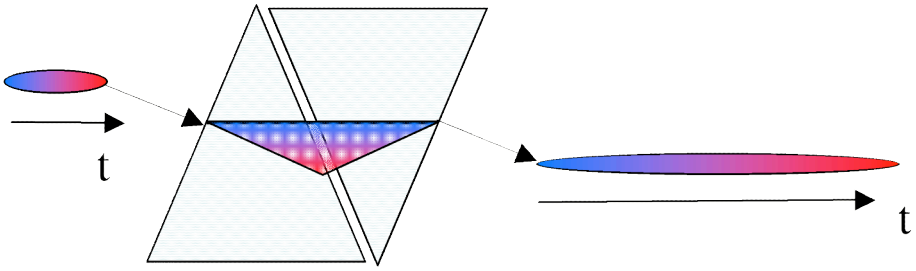

Fig. 3.c.3 A chirped FEL pulse can be extended using an optical system with a pass-time depending on the wavelength.

Overall, the ERL-based FEL can meet all requirements for the driver of a polarized electron gun with average current of 0.5 A. Being based on exactly the same elements as those used for 10 GeV ERL, this laser source can be build within a very modest budget.

References:

[3.c.1] G.Neil et al., Phys. Rev. Letts. **84**, 662 (2000)
[3.c.2] http://www.cebaf.gov/FEL/feldescrip.html
[3.c.3] V.N.Litvinenko et al., NIM **A 475** (2001) 247-252
[3.c.4] V.N.Litvinenko et al., NIM **A 475** (2001) 407-416
[3.c.5] H.Hama et al., NIM **A 393** (1997) 23
[3.c.6] N.A.Vinokurov, A.N.Skrinsky, Preprint 77-59, BINP, Novosibirsk (1977)
[3.c.7] V.N.Litvinenko et al., NIM **A 475** (2001) 65-73

3.d e-beam polarization and polarization transparency of the ERL lattice

In remarkable contrast with many other schemes, the ERL option for the eRHIC does not have any forbidden energy ranges[12], and a desirable polarization of electrons can be maintained at any energy of electrons without using spin-matching sections or "snakes".

This flexibility and the spin-transparency of the ERL are most evident in the present ERL scheme shown in Fig. 3.d.1. By design, the electron trajectory stays in the horizontal plane from the gun to the IP and, therefore, the spin also stays in the horizontal plane, x-z.

Electrons are generated in a photo-injector with longitudinal polarization exceeding 80% (see section 3.b) and the energy of $E_i = \gamma_i mc^2$. Helicity (projection of spin on the momentum, i.e., the z-axis) is controlled by choosing the helicity of the photons, and can be switched from positive to negative. The electron beam is turned for the angle $\theta_i = \pi/12$, and is injected into first stage of the ERL. This stage has one linac. The electron beam passes twice through it gaining $\Delta E_1 = \Delta\gamma mc^2$ at each pass, and then makes one 360° turn before reaching transfer energy $E_1 = \gamma_1 mc^2$ in the second section of the ERL. The e-beam makes $\theta_t = \pi/2$ turn before reaching the first main acceleration section.

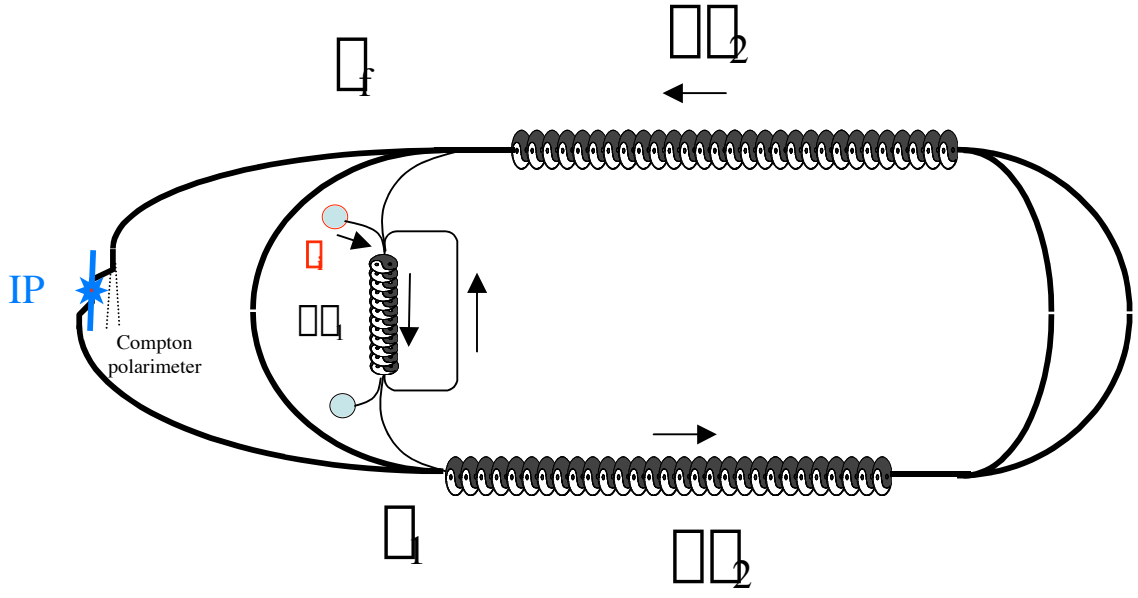

Fig.3.d.1. Acceleration scheme for eRHIC with a two-pass ERL

[12] To be exact, it is correct for all energies of interest for eRHIC. This scheme would not work for very low energies of electrons $E_f < 0.22$ GeV.

The second stage of the ERL is comprised of two linacs, and electron beam passes twice through each of them gaining $\Delta E_2 = \Delta\gamma_2 mc^2$ at each pass, and makes three180 turns before reaching final energy $E_f = \gamma_f mc^2$. The e-beam makes its last $\Delta\theta_t = \pi/2$ turn before reaching its goal in the IP.

After the IP, polarization of the electrons in no longer important and downstream of it, the lattice does not need to be "spin-transparent".

It is important to notice that acceleration along z-axis does not affect the particles' spin[13]. Therefore, spin rotation occurs only in the bending magnets. The vertical magnetic field in the arcs turns the trajectory of the electrons and rotates their spin about the y-axis for an angle, $\Delta\Psi$, proportional the angle of trajectory rotation, $\Delta\theta$, electron energy $E_e = \gamma mc^2$, and the anomalous magnetic moment, $a = g/2 - 1 = 1.1596521884 \cdot 10^{-3}$:

$$\Psi = \frac{g}{2}\frac{e}{m_o}\hat{s} = (1+a)\frac{e}{m_o}\hat{s}; \qquad \Psi_{spin} = a\cdot\theta = \frac{E_e}{0.44065[GeV]}$$

$$\Delta\Psi = \Delta\theta \cdot \gamma \cdot a. \tag{3.d.1}$$

Therefore, the total angle of spin rotation is a direct sum of the individual turns (see below):

$\Delta\Psi/\pi$	γ
-1/12	γ_0
2	$\gamma_0 + \Delta\gamma_1$
1/2	$\gamma_0 + 2\Delta\gamma_1$
1	$\gamma_0 + 2\Delta\gamma_1 + 1\Delta\gamma_2$
1	$\gamma_0 + 2\Delta\gamma_1 + 2\Delta\gamma_2$
1	$\gamma_0 + 2\Delta\gamma_1 + 3\Delta\gamma_2$
1/2	$\gamma_0 + 2\Delta\gamma_1 + 4\Delta\gamma_2$

and for the entire pass from one can easily calculate the total angle of the spin rotation:

$$\Psi = a\sum_k \Delta\theta_k\gamma_k = \pi a\{(6-1/12)\gamma_i + 10\Delta\gamma_1 + 8\Delta\gamma_2\}. \tag{3.d.2}$$

The final energy of electrons

$$\gamma_f = \frac{E_f}{mc^2} \equiv \gamma_i + 2\Delta\gamma_1 + 4\Delta\gamma_2; \tag{3.d.3}$$

---

[13] According to Bargman, Mitchel, and Telegdi's equation, in the absence of magnetic field

$$\frac{d\hat{s}}{dt} = \frac{e}{mc}\hat{s}\times\left[\left(\frac{g}{2}-1+\frac{1}{\gamma}\right)\vec{B} - \frac{\gamma}{\gamma+1}\left(\frac{g}{2}-1\right)\hat{\beta}\left(\hat{\beta}\cdot\vec{B}\right) - \left(\frac{g}{2}-\frac{\gamma}{\gamma+1}\right)\vec{\beta}\times\vec{E}\right]$$

particle spin is preserved for a particle moving along electric field $\vec{\beta}\,//\,\vec{E}$.

is defined by the experiment. Usually fixing the injection energy is required by conditions for generating very bright electron beam. These make the choice of energy gains in the ERL linac unique for longitudinal polarization in the IP[14]:

$$\Delta\mathcal{E}_2 = \frac{\mathcal{E}_f - \mathcal{E}_i}{4} - \frac{\Delta\mathcal{E}_1}{2}$$
$$\frac{\mathcal{E}}{m} = a \cdot \left[\frac{47}{12}\mathcal{E}_i + 2\mathcal{E}_f + 6\Delta\mathcal{E}_1\right] = N \qquad (3.d.4)$$

where N here is an integer number. Chousing N to be nearest integer to the nominal energy gains (required for reaching the final energy)

$$N = \text{nearest\_integer}\left[a\left(\frac{47}{12}\mathcal{E}_i + 2\mathcal{E}_f + 6\Delta\mathcal{E}_{1\,\text{minimal}}\right)\right]$$

and using a small adjustment of $\Delta\mathcal{E}_1$

$$\Delta\mathcal{E}_1 = \frac{1}{6a}\left(\frac{\mathcal{E}}{m}\right) - N\left] \approx 143.7 \cdot \left(\frac{\mathcal{E}}{m}\right) - N\right]$$

provide for integer number of π-rotation for electron spin. In the above scheme, a very small adjustments of the linacs in two sections in the range of

$$\Delta\mathcal{E}_1 \in \{-71.9, 71.9\}; \quad \Delta E_{linac1}[MeV] \in \{-36.72, 36.72\}$$
$$\Delta\mathcal{E}_2 = -\Delta\mathcal{E}_1/2; \quad \Delta E_{linac2} = -\Delta E_{linac1}/2$$

do provide for attainment of complete spin transparency[15]. It is advantageous for the beam stability to operate fist section of ERL close to nominal accelerating gradients. Presently the nominal ranges for the ERL with two passes[16] are shown in next table:

Injection energy	5	MeV
E_1	1000	MeV
Final	2-10	GeV
Nominal ΔElinac1	497.5	MeV
Nominal ΔElinac2	1000 - 2250	MeV
Nominal $\Delta\mathcal{E}_1$	973.58	π
Nominal $\Delta\mathcal{E}_2$	489 - 4403	π

[14] First, capability of spin flip at the source side allows us to have integer number of 180° turns of spin. Proper helicity is chosen at the gun. Conditions similar to (3.d.4) can be derived for any plane ERL [3.d.1].

[15] It is important to note that initial energy spread of electrons is very small $\sigma_\delta \ll 1$. The energy spread is kept small $\sigma_\delta < 1$ (see section 3.a) also during the acceleration process. Therefore, the spread of the spin rotation angle caused by the energy deviation stays very small $\sigma_\theta < 7a\sigma_\delta \approx 0.025$ *rad*, $\cos\sigma_\theta \approx 0.9997$ and high degree of e-beam polarization is preserved.

[16] Energies of electron beam from 2 GeV to 5.5 GeV can be reached with a single pass through the ERL linacs, which is a preferable choice.

The process of making the lattice spin-transparent at *any energy of operation* is as simple as following:

- ✓ Energy gain in the first and second linac are slightly adjusted (for less than 40 MeV) to satisfy criteria (3.d.4) while keeping final energy fixed.

An example of the choice for accelerating gains of two linacs for e-beam energy range from 5 to 10 GeV is shown in Fig.3.d.2

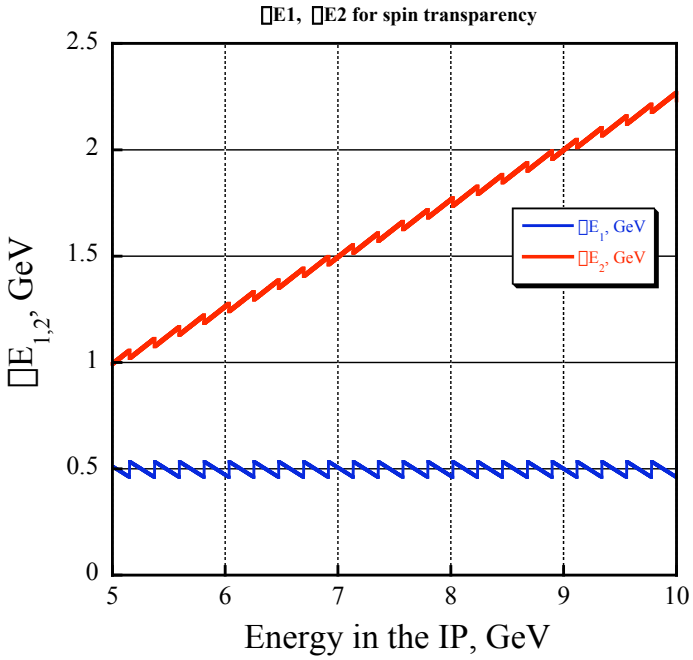

Fig. 3.d. Required energy gains for spin transparency vs. the e-beam energy in the IP.

Similarly the spin transparency can be kept with a single pass ERL (see Fig. below).

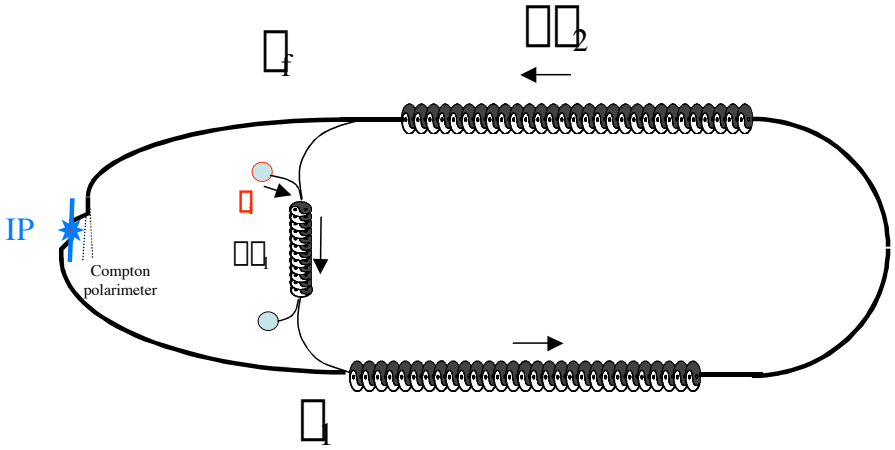

Fig.3.d.3. Scheme for low energy eRHIC operation with a single-pass through ERL.

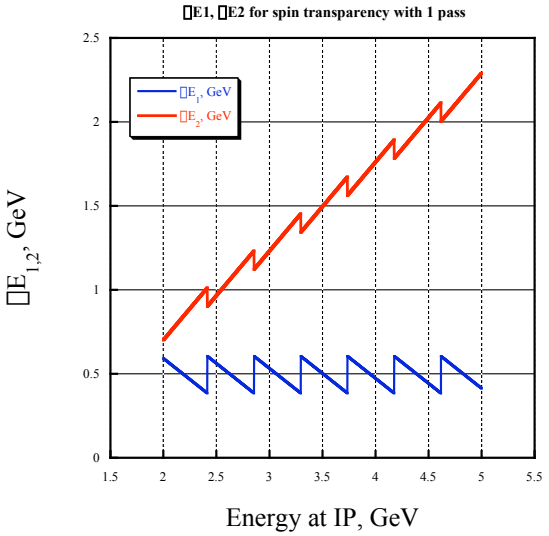

Fig.3.d.4. The choice of the energy gains for linacs for a single - pass through the ERL

In addition to longitudinal polarization by a properly selecting energy gains in two linacs of ERL, e spin can be oriented horizontally in the IP, if required. Overall, the ERL-based eRHIC has full capability of controlling the polarization of electrons in the IP while preserving a very high degree of polarization attained at the photo-cathode. Most importantly, there are several schemes with ERL-based eRHIC that allow *any desirable polarization at the IP at any desirable energy of electrons*. The scheme described in this section is one of them.

References:

[3.d.1] V.N. Litvinenko, W.W. Mackay, I.Ben-Zvi, "Spin Transparency of ERL lattice", C-AD internal note

3.e Electron cooling

In this section, we focus on issues specific for the ERL-based eRHIC, which allows operation with double the intensities of both the ion- and proton-beams compared with ring-ring option [3.e.2]. Electron cooling plays as important a role in the ERL-based eRHIC as it does in the ring-ring case.

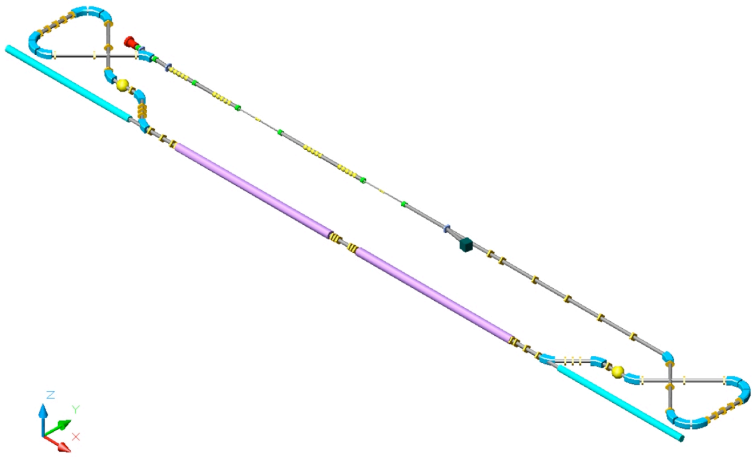

Fig. 3.e.1. eRHIC electron-cooler system comprises a photoinjector (red), a superconducting energy-recovery linac, and a cooling RHIC section with 30-m long solenoid (purple).

The detailed description of electron-cooling scheme (fig.3.e.1) and its aspects specific for eRHIC operation are shown in Section 3.2.1 in the main body of ZDR [3.e.1]. To achieve the design luminosity of eRHIC, an ion beam must be continuously cooled while colliding with the electron beam. The needs for electron cooling in eRHIC can be summarized as the following:

1. The RHIC gold-beam evolution is dominated by Intra-Beam Scattering (IBS) that leads to the growth of emittance and beam loss and/or de-bunching. Electron cooling is planned during the storage phase of the machine to control IBS and reduce emittance to the required values (limited by the beam-beam parameters).
2. For high-energy 250 GeV protons, electron cooling is ineffective. This suggests a staged cooling for such protons: they are initially cooled at injection energy with a subsequent acceleration to higher energy. At low proton energies in the range of 25-50 GeV, using cooling reduces transverse-beam emittance to the required values.
3. Cooling the longitudinal emittance causes bunch shortening at both low- and high-energies, and, hence, provides the match with a low β^* in the IPs.

Initial simulations indicate that all the major tasks described above can be achieved with the electron cooler presently under design for the RHIC II upgrade. Section 3.2.1 presents the simulations of cooling times for the current eRHIC baseline intensities

of protons (Np=1x10^{11}) and Au ions (Ni=1x10^{9}). Here we offer some examples for upgraded intensities of the RHIC beams to N_p=2x10^{11} and N_i=2x10^{9} for protons and Au ions per bunch.

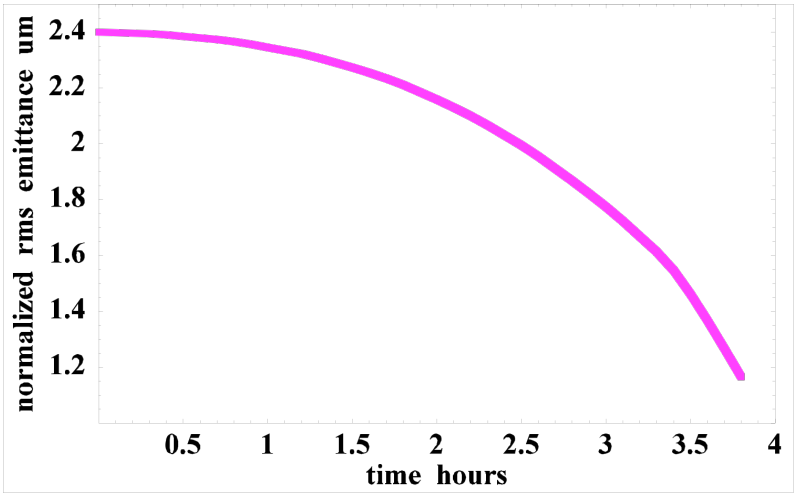

Fig.3.e.2 BetaCool simulation code: Cooling of a proton bunch with N_p=2x10^{11} 27 GeV protons to a normalized rms emittance of 1.2 □m.

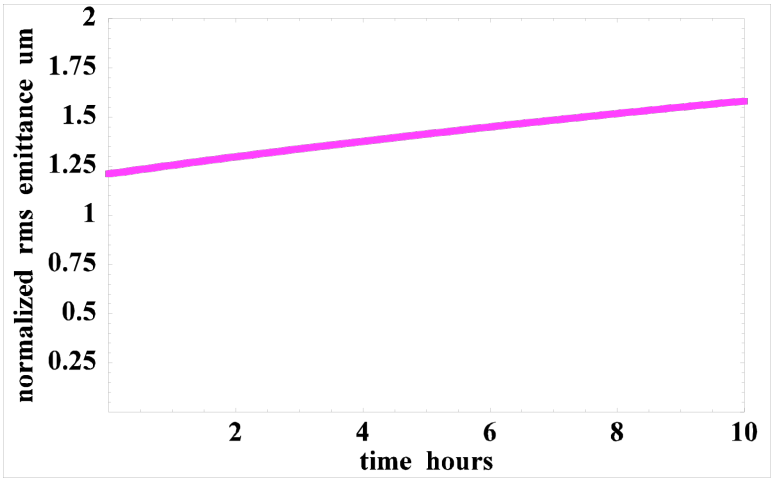

Fig.3.e.3. . BetaCool simulation code: Emittance growth of the cold proton bunch with N_p=2x10^{11} particles stored at 250 GeV.

For high-intensity protons, staged cooling is employed. The protons are first cooled at energy of 27 GeV, and then accelerated to the energy of experiment. Figure 3.e.2 shows cooling of protons (N_p=2x10^{11}) using a current of electron cooler corresponding to the number of electrons in a bunch Ne=1x10^{11} (16 nC per bunch). Figure 3.e.3 shows emittance growth via IBS of the cold proton beam accelerated and stored at 250 GeV for 10 hours. Overall, the simulations support the possibility of

maintaining the beam's quality of intense protons required for attaining $2x10^{33}sec^{-1}cm^{-2}$ luminosity in theERL-based eRHIC.

Electron cooling also is essential for reaching the design luminosity of $2x10^{31}$ sec^{-1} cm^{-2} in e-Au collisions with 100 GeV/u golden ions. As discussed previously, this requires an intense ion beam with $2x10^{9}$ ions per bunch. Without cooling, both the transverse and longitudinal emittance of such a beam will increase very rapidly because of IBS. This would cause the luminosity to decline, and/or particle loss from the bucket due to bunch lengthening. Fig.3.e.4. is a simulation of this scenario (no-cooling!).

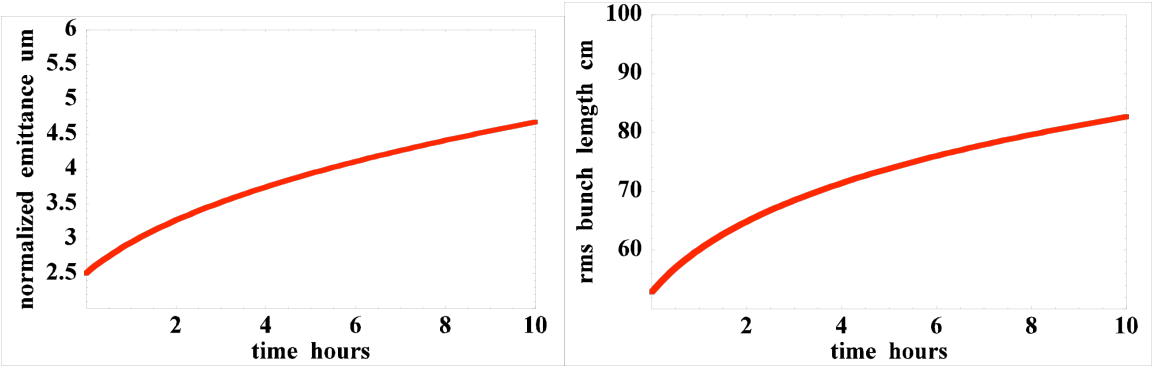

Fig.3.e.4. BetaCool code- WITHOUT COOLING!: Growth of transverse normalized rms emittance (left) and rms bunch length due to the IBS for 100 GeV/u Au ions beam with $2x10^{9}$ particles per bunch.

Electron cooling changes the situation rather dramatically: with $2x10^{9}$ ions per bunch, it cools down the longitudinal emittance while maintaining the transverse emittance required for $2x10^{31}$ $sec^{-1}cm^{-2}$ luminosity. It is noteworthy that this result is based on typical cooler parameters (see Section 3.2.1). Figs. 3.e.5 and 3.e.6 illustrate this mode of eRHIC operation.

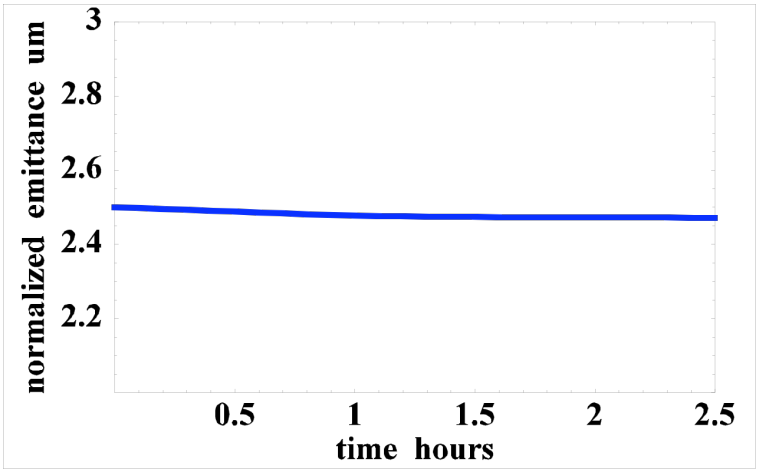

Fig.3.e.5. BetaCool code: Time evolution of rms emittance for a 100 GeV/u Au ions beam with $N_i=2x10^{9}$ particles per bunch. The electron current of the electron cooler corresponds to $N_e=1x10^{11}$ per bunch.

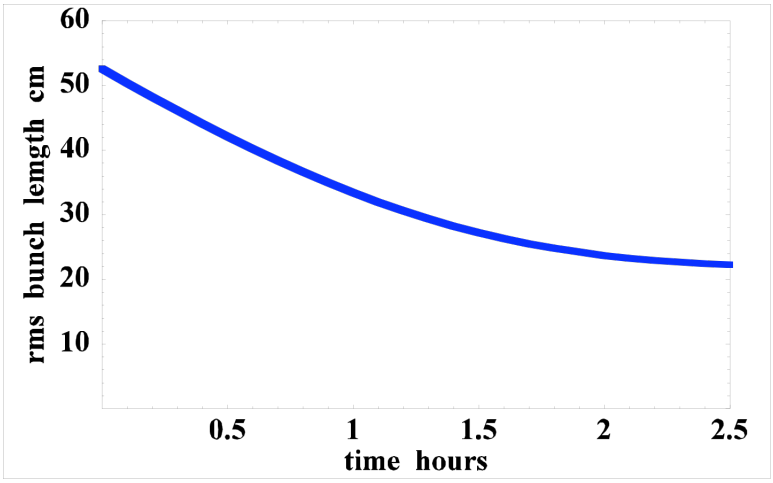

Fig.3.e.6. BetaCool code: Time evolution of the rms bunch length of a 100 GeV/u Au ions bunch with $N_i=2x10^9$ particles. The electron cooler's parameters are the same as in Fig. 3.e.5.

Overall, the simulations provide confidence in the feasibility of high luminosity levels for eRHIC ($2x10^{33}sec^{-1}cm^{-2}$ and $2x10^{11}sec^{-1}cm^{-2}$ for e-beam collision with 250 GeV protons and 100 GeV/u gold ions, correspondingly).. In addition, there is an opportunity to further "luminosity-relevant" electron cooling by fast cooling of ion-beam core by adjusting the size of the transverse electron beam in the cooling section.

As the part of preparing for electron cooling of RHIC beams, R&D on a several systems relevant to the eRHIC is underway: the photoinjector (including its laser and photocathode deposition system), a high-current superconducting cavity for the ERL of the cooler, beam dynamics of the complete system, electron cooling simulation codes, and the high-precision superconducting solenoid.

Electron cooling is important integral part of the linac-ring eRHIC. It provides for the attainment of low emittances required for high luminosity of the linac-ring eRHIC. In addition it provides flexibility of further reducing emittance of hadron beams for extending luminosity towards $10^{34}sec^{-1}cm^{-2}$ per nucleon or for compensating for reduced intensity of the hadron beam.

References:

[3.e.1] ZDR section 3.2.1: Electron Cooling for eRHIC, I. Ben-Zvi, A. Fedotov, J. Kewisch, V.Litvinenko

[3.e.2] ZDR section 1.2: General accelerator concept and parameters V.Ptitsyn, T.Roser et al.

3.f Integration with IP

The interaction region of eRHIC collider serves several purposes. Firstly, both the hadron- and electron-beam should be focused into an optimally equal size at the IP(s) to maximize luminosity. Secondly, there should be sufficient convenient space and volume for the detector to conduct the physics experiments. Thirdly, the apertures and the environment for the beams should provide both for the low experimental background and long luminosity lifetime.

The ERL-based eRHIC has a number of significant advantages for integrating the IP(s):

- ✓ Round-beam collision geometry to maximize luminosity
- ✓ Smaller e-beam emittance resulting in 10-fold smaller aperture requirements for the electron beam
- ✓ Possibility of moving the focusing quadrupoles for the e-beam outside the detector and the IP region, while leaving the dipoles used for separating the beam.
- ✓ Possibility of further reducing the background of synchrotron radiation.

Within this scheme, the first hadron low-β quadrupole, Q1, is installed at 5m from the IP. This requires deflecting the electrons sufficiently to guide them through a field-free region outside this magnet. Since this separation generates synchrotron radiation, it is mandatory to keep it as small as possible by installing septum quadrupoles for the hadron beam.

To minimize the actual volume of the detector occupied by the separation magnets, superconducting dipole magnets are foreseen, similar to those in the HERA luminosity upgrade design [3.f.4]. These dipoles deflect the electron beam while leaving the higher-energy hadron beam's orbit practically unchanged.

3.f.2 Electron beam in the IP [3.f.2]

The tune-shift limitations and the aperture requirements for hadron beams in the ERL-based eRHIC are identical to those in the ring-ring scenario [3.f.1]. At the same time, for the ERL-based eRHIC, the tune shift for electrons can be very large $\Delta Q_e \sim 1$ compared with the ring-ring case. The effect of the collision on the electron beam is better described by disruption parameter (see chapter 2):

$$D = \frac{Z_h N_h}{\sigma_e} \frac{r_e}{\sigma^2_{r(h)}} \sigma_{s(h)};$$

that essentially is a betatron phase advance in the e-beam caused by the hadron beam.

Our studies [3.f.2] revealed that with proper matching in the ERL case, tune shifts up to $\Delta Q_e = 1$ (i.e., disruption parameters up to ~2π) only modestly increase the beam's emittance by ≤ 20%. An electron beam with such emittance can be easily re-circulated in the ERL down to the beam damp.

Fig. 3.f.1(a,b) illustrates one example of the effect of an intense hadron beam on the electron beam. The RMS emittance of the hadron beam (100 GeV/u golden ions) is intentionally reduced from 9.4 nm.rad to 5 nm.rad (RMS normal emittance!) to increase the effect on the electron beam by a factor of ~ 1.9. This is also the reason for the reduced e-beam betatron function in the IP, which is required for fitting the e-beam and ion beam sizes in the center of the IP (z=0 in Fig/ 3.f.1b). The situation is even better for luminosity of $4 \cdot 10^{33}$ cm^{-2} s^{-1} per nucleon (i.e., 9.4 nm.rad RMS emittance of hadron beam).

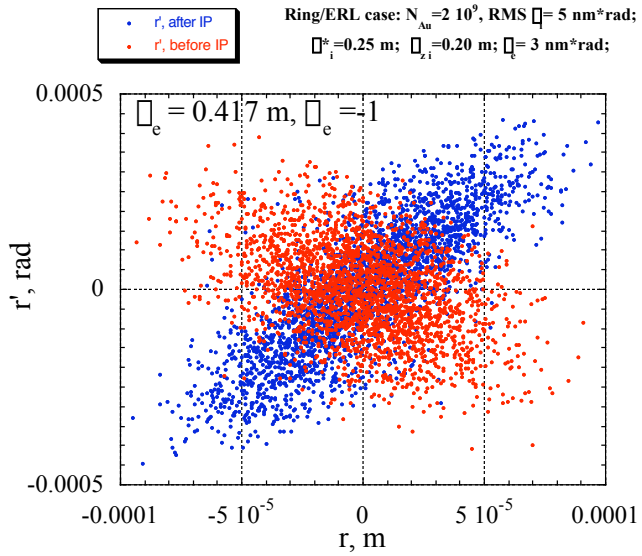

Fig. 3.f.1a Round 10 GeV electron beam from ERL with initial transverse RMS emittance of 3 nm·rad passes through the IP with the disruption parameter 3.61 (tune shift $\Delta Q_e = 0.6$). Figure shows Poincare plots for e-beam distribution before (red) and after (blue) the IP. After removing the *r-r'* correlations, the emittance growth is only 11%.

Another effect, which is of concern for the hadron beam, is a modulation of the size of the electron beam during the collision. Our simulation showed that these variations can be controlled at least for luminosity ~10^{34} cm^{-2} s^{-1} per nucleon for gold-electron collisions (see figure below). For the parameters listed in Table 2.1, the beam-modulation effect is lowered by an additional factor of 4 compared with this figure.

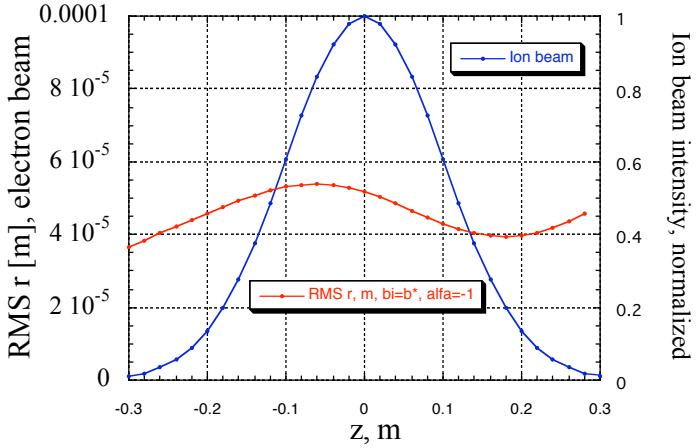

Fig. 3.f.2 Round electron beam from ERL with an initial transverse RMS emittance of 3 nm*rad passes through the IP with the disruption parameter 3.61 (tune shift ξ_e = 0.6). Matching the beam's size with the ion beam and a negative β=-1 at z=-0.3m, permits a modest variation of the e-beam's size (red line on the right graph) through the interaction region; the e-beam's size does not shrink below the matched value. In this case, the tune shift for hadrons does not exceed ξ_h = 0.005.

Another effect, the kink head-tail instability of the hadron beam, and its stabilization were considered in section 2.

Overall, there appears to be no problem in using electron beams above 5 GeV in ERL-based eRHIC within the luminosity ranges ~ 10^{34} cm^{-2} s^{-1} per nucleon.

3.f.2 Hadron IR optics [3.f.1]

One of the main advantages of the linac-ring eRHIC vs. ring-ring eRHIC is operating the IP with round beams. The ring-ring case requires hadron optics with flat beams and unequal β^*: β_x =1.04 m, β_y = 0.26m. In the case of the linac-ring , the hadron beam is round with β^*=0.26m in both directions. A normal-conducting quadrupole triplet focuses the hadron beam in the IP region.. The use of septum-quadrupoles for all these magnets minimizes the required beam separation between electrons and hadrons, and affords maximum freedom for installing magnets in the electron beam's line.

The first and second lens of the triplet are split up into various individual magnets, with pole tip radii tailored to the varying beam size. This ensures a sufficient aperture of 12σ_p, while simultaneously minimizing the total length of the low-β system. Figure 3.f.1 illustrates the resulting β functions and magnet positions.. Whenever possible, pole tip fields were limited to 1.0T to avoid degradation in field quality due to saturation. However, in most magnets this limit had to be exceeded slightly to accommodate the 12σ_p beam in the septum quadrupoles. Table 3.f.2 lists the resulting magnet parameters, while cross-sections of the entrance and exit of each magnet with its pole tip radius and the 12σ_p beam ellipse are shown in Figures 3.f.3 and 3.f.4.

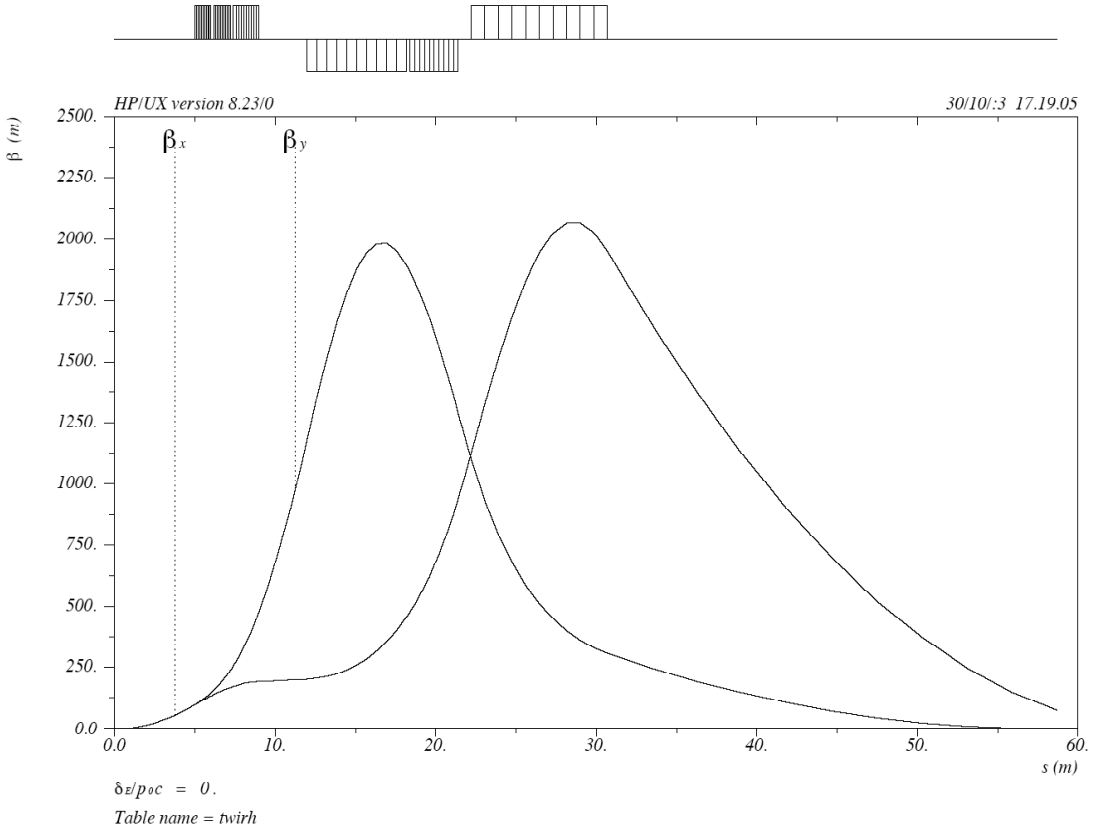

Figure 3.f.2: Hadron IR lattice for the electron-ion collider eRHIC

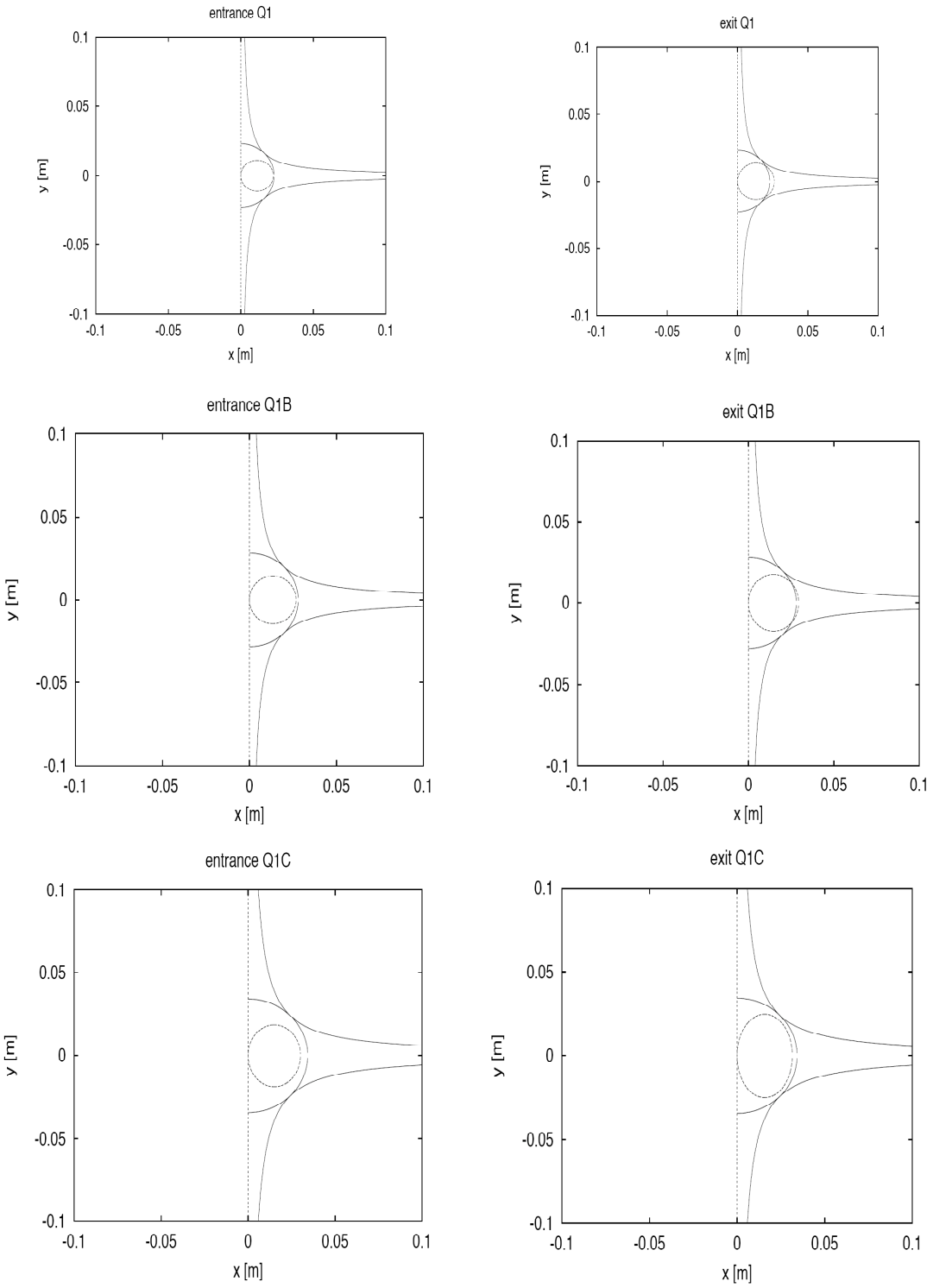

Fig. 3.f.3. Hadron beam envelope, magnet pole-tips, and vacuum chamber in the first hadron magnet Q1 comprising three parts [3.f.3].

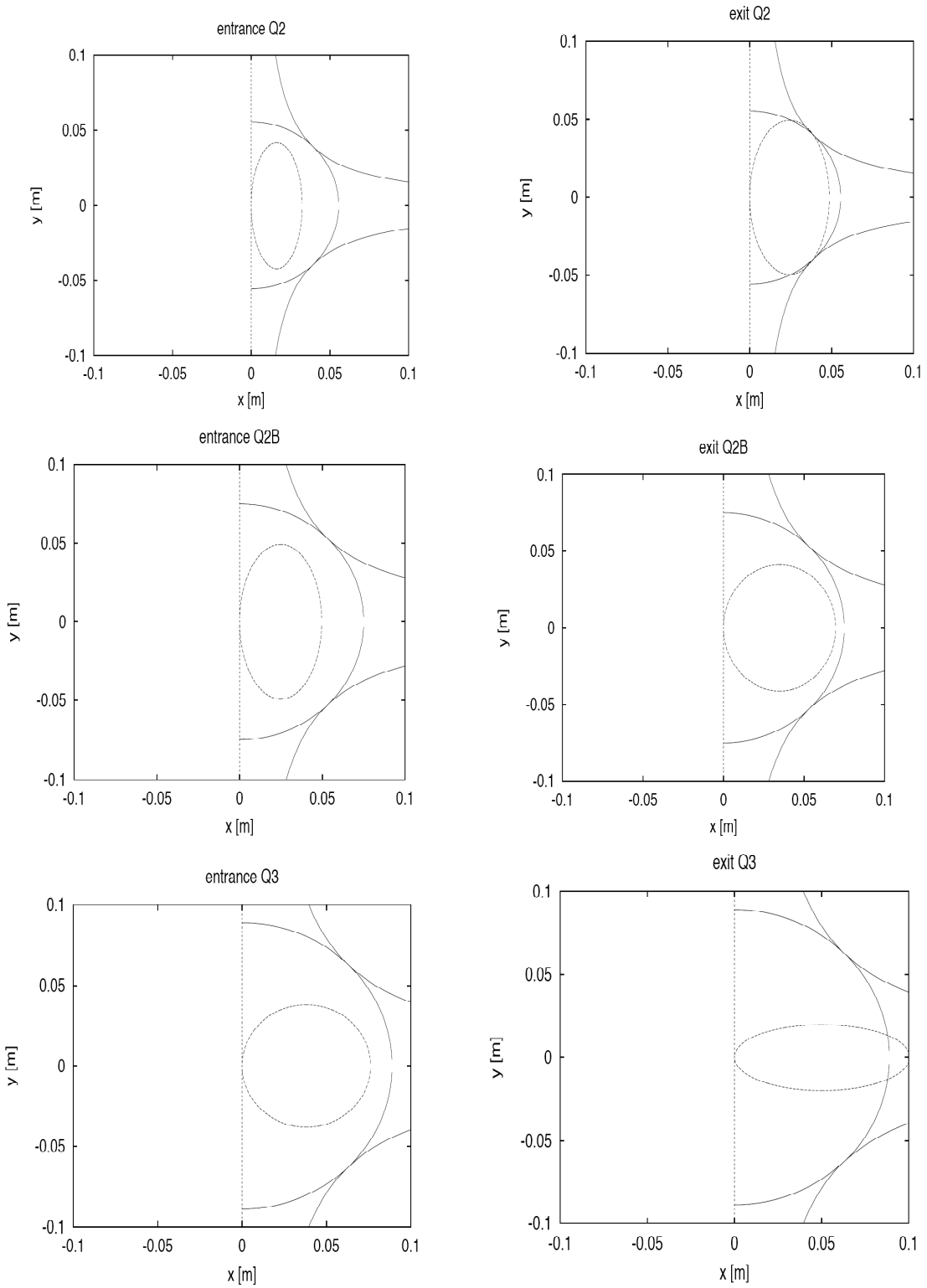

Fig. 3.f.4. Hadron beam envelope, magnet pole-tips, and vacuum chamber in the second and third hadron magnet Q2-Q3 [3.f.3].

Table 3.f.1: Parameter list of the hadron low-β septum quadrupoles

	Q1	Q1B	Q1C	Q2	Q2B	Q3
length [m]	1.0	1.0	1.6	6.2	3.0	8.5
gradient [T/m]	43.5	35.7	29.2	18.0	13.3	11.3
pole tip radius [mm]	26.4	30.8	37.7	61.1	75.0	88.9
pole tip field [T]	1.15	1.1	1.1	1.1	1.0	1.0

3.f.3 Synchrotron radiation [3.f.3].

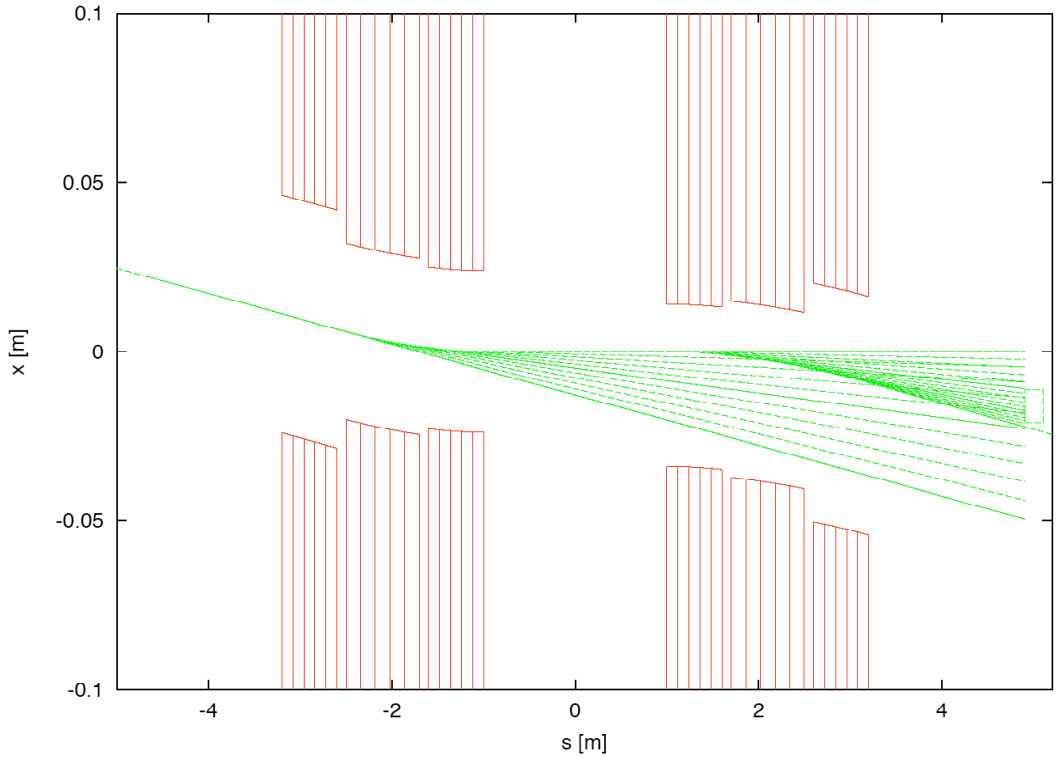

Figure 3.f.5: IR geometry and synchrotron-radiation fan. The electron beam enters the IR from the left. A box on the right indicates the septum of the Q1 magnet.

The synchrotron-radiation fan results from the superconducting dipole windings necessary to separate the beam. At the septum, 5m from the IP, the required separation is given by the $12\sigma_{p,x}$ beam size of the hadron beam, plus the thickness d_{septum} = 10mm of the septum itself, plus some sufficient aperture for the electron beam. In contrast to the ring-ring case, where $20\sigma_{e,x}$ are mandatory for sufficient lifetime of the electron beam and minimum background conditions, this condition is much more relaxed in the linac-ring approach for two reasons. First , an aperture of 5 $\sigma_{e,x}$ is adequate , where the beam passes through the interaction region only once and the halo is absent. Second, the horizontal electron-beam's emittance is more than an order-of-magnitude smaller. Using

the 2.5 nm RMS e-beam emittance the RMS e-beam's size can be less a quarter of mm throughout the IP. Using the β-functions shown in Figures 3.f.2 for the hadron beam with RMS emittance of 9 nm·rad, the required separation is computed as[17]

$$\Delta x = 12\sigma_{p,x} + 5\sigma_{e,x} + d\text{septum} = 12\cdot 0.93\text{mm} + 5\cdot 0.25\text{mm} + 10\text{mm} = 22.4\text{mm}.$$

At the right side of the detector (electron-downstream), some fraction of this fan always hits the septum of the first hadron quadrupole, Q1. To minimize back-scattering of these synchrotron-radiation photons into the detector, the total power as well as the critical photon energy of the synchrotron radiation hitting the septum must be minimized by distributing the required bending angles among the various magnets. The distribution of the synchrotron radiation in and around the IP can be optimized by properly distributing the separating magnetic field. Table below lists some parameters of three separating magnets used for generating the synchrotron radiation fan shown in Fig.3.f.5.

Table 3.f.2: Selected parameter of separating magnets from both sides of the IP

	B1,left/right	B2, left/right	B3, left/right
length [m]	0.6/0.6	0.8/0.8	0.6/0.6
bending angle [mrad]	3.7/-3.0	3.8/-2.4	3.75/-3.6
synchrotron radiation power [W]	1609/1058	1273/508	0/677
synchr. rad. power on septum [W]	800/0	0/508	0/340
critical photon energy [keV]	13.7/11.1	10.5/6.7	0/8.9

The eRHIC interaction region discussed above provides for an e-p luminosity of $2\cdot 10^{33}$ cm^{-2} sec^{-1} with hadron beam-beam tune shift of $\Delta_{x,y} = 0.005$, which is well within values presently achieved at RHIC, and therefore, considered achievable for eRHIC. Minimum apertures of $12\sigma_{p,x}$ for the hadrons are possible in this design that is considered sufficient both for safe operation as well as for minimum detector background conditions.

References:

[3.f.1] eRHIC ZDR, Main part, Chapter 3.

[3.f.2] I.Ben-Zvi, J.Kewish, V.N.Litvinenko., ICFA Beam Dynamics Newsletter No. 30, April 2003, p.19

[3.f.3] DESIGN OF AN INTERACTION REGION FOR THE LINAC-RING VERSION OF THE ELECTRON-ION COLLIDER ERHIC, C. Montag, J. Kewisch, I. Ben-Zvi, Internal Technical Note, C-AD

[3.f.4] U. Schneekloth (ed.), The HERA Luminosity Upgrade, DESY HERA 98-05

[17] It might be possible to use a significant vertical separation of the superconducting dipole windings in the detector that would allow the synchrotron-radiation fan to be passed safely outside the system.

3.g Considerations of the experiments

There is a strong desire in the physics community for eRHIC to have at least two IPs and for potential of multiple IPs. The linac-ring eRHIC has such options naturally incorporated into its design. Using the electron form ERL provides for additional experimental possibilities such running two experiments with different energies of electron in different IPs, or for arbitrary split of the luminosity between different detectors[18].

Using low emittance electron beam in linac-ring eRHIC provides for significant simplifications of the final focusing optics (see previous section). Specifically, it provides for possibility of moving all focusing optics for electron beam as far as 10 meters outside of interaction region. This is an advantage for experimental set-up- a detector has a very long straight section free from accelerator elements for its installation. This configuration fits most naturally with a long low-x detector with magnetic field [3.g.1].

According to the HERA experience, synchrotron radiation in the IP can be a main source of background. The linac-ring eRHIC provides the possibility of reducing the intensity of the this background while keeping high luminosity very high (see the introduction).

Overall, very high luminosity added by flexibilities provided in linac-ring eRHIC will be a very significant asset for installation of effective detectors for the most aggressive physics program [1].

References

[3.g.1] "A new detector concept for e-p physics", I. Abt, presented at eRHIC Meeting at BNL January 29-31, 2004

[18] Note that in linac-ring eRHIC luminosity can be split between various detectors and is only limited to a total value ~ 10^{34} sec^{-1} cm^{-2} per nucleon.

3.h Adjustment of collision frequency for variable proton- and ion- energies

Operating the eRHIC requires various energies of hadrons from 26 to 250 GeV/u ($27 < \gamma_h < 267$) that causes a significant variation in the revolution frequency in the RHIC, and hence, variations in the hadron beam's repetition rate in the IP:

$$f_o = \frac{C_{RHIC}}{v_h} \approx \frac{C_{RHIC}}{c}\left(1 + \frac{1}{2\gamma_h^2}\right), \quad f_{rep} = N_b \cdot f_o \approx 28 \ MHz$$

where C_{RHIC} is the circumference of RHIC ring and $N_b=360$ is the number of hadron bunches in the eRHIC. By definition, the electron beam's repetition rate must be the same as that of the hadrons. Within the entire range of foreseen eRHIC operations, electrons remain ultra-relativistic ($\gamma_e > 4{,}000$) and their velocity is practically constant ($0 < 1 - v_e/c < 3.2 \cdot 10^{-8}$). Covering the 26 - 250 GeV/u hadron-energy range will require adjusting the e-beam rep-rate within

$$\frac{\Delta f_{rep}}{f_{rep}} \approx 0.7 \cdot 10^{-3}.$$

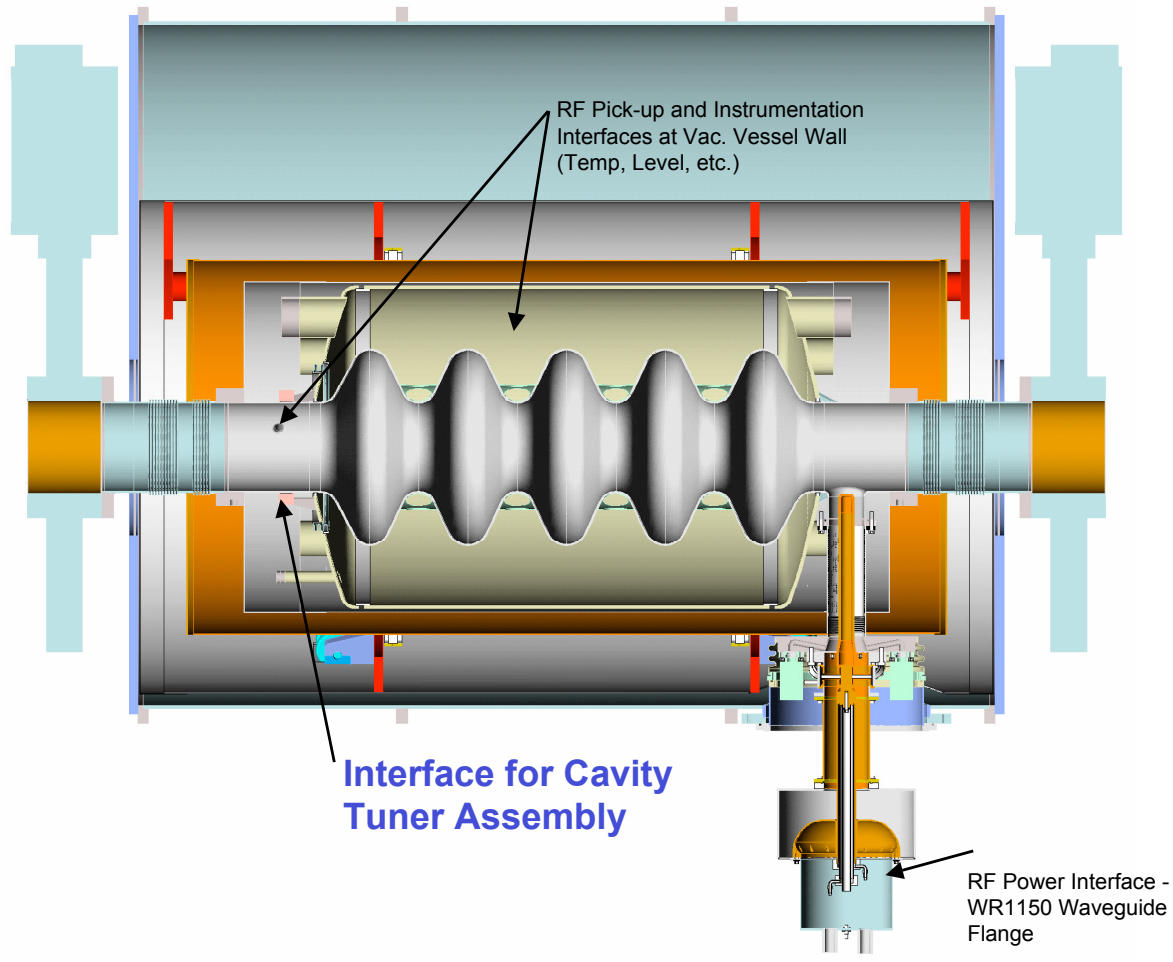

Fig. 3.h.1 A five-cell superconducting cavity with its tuning mechanism.

In contrast to the ring-ring version of eRHIC, where the above requirement is translated into the need for changing the circumference of the electron storage ring by about 0.9 m and causes significant modification of the lattice [3.h.1], in the ERL-based eRHIC it does not raise significant difficulties.

First, in the ERL the repetition rate of the electron beam is controlled by the RF frequency of the superconducting accelerating structure (see below), which operates at 25^{th} harmonic of the beam rep-rate in the eRHIC ($f_{SCC} \sim 705\ MHz$). This cavity is being developed [3.h.2] and is designed to have tunability at least $\Delta f / f \sim 1 \cdot 10^{-3}$, thereby exceeding the above requirement by a wide margin.

The following features of the ERL ensure proper phase matching of the electron beam with each accelerating cavity of the ERL:

- The accelerating structures in each of three linacs will have an individual phase tuner for compensating for the varying RF frequency

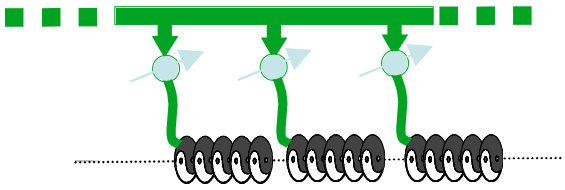

Fig. 3.h.2. A phase tuner controls the phase of each individual cavity.

- The phases of three individual linacs will be individually controlled in conjunction with five chicanes in the arcs and turns;
- The lattice of the ERL arcs is very relaxed and they need to be adjusted by less than a half RF wavelength (λ_{RF}=0.425m, i.e., ΔL<0.215m) using low- and medium-energy chicanes installed in the straight section with large R.
- There is no chicane in arcs at the maximum energy – the phasing is provided by the linacs.

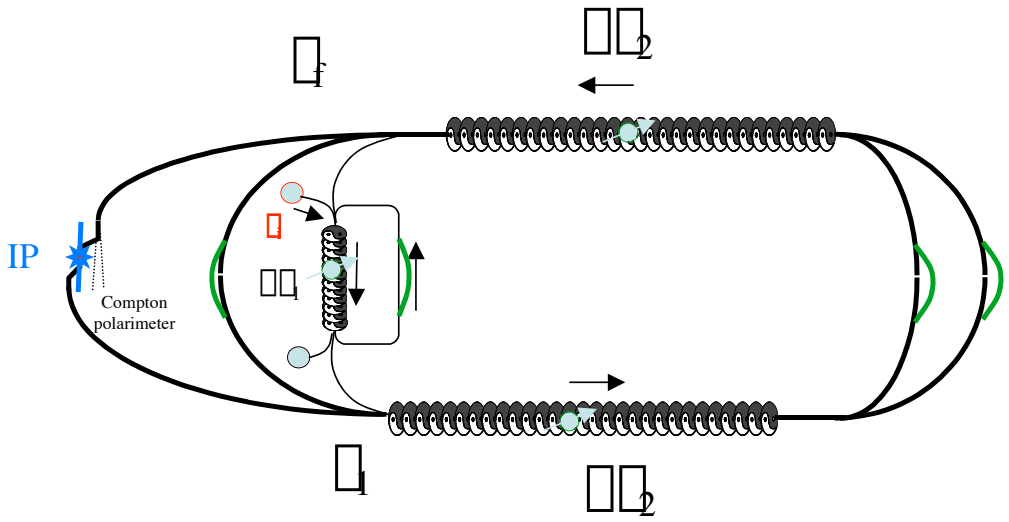

Fig. 3.h.2. The phase matching of the entire ERL system is assured by the phase control of three linacs and four chicanes (depicted by green lines) at intermediate energies.

Overall, the ERL-based eRHIC can comfortably adjust the e-beam repetition rate to any of designed energies of the hadron beam.

References:

[3.h.1] C. Tschalaer, Ring path length adjustment, Presentation at eRHIC Collaboration Meeting, August 19-20, 2003 , BNL, http://www.agsrhichome.bnl.gov/eRHIC/

[3.h.2] I. Ben-Zvi et al., High current SCC

4. Cost

The cost of the ERL-based eRHIC should be close to that of the superconducting linac injector for the ring-ring eRHIC. The main differences will be in following components

- 2 K^o refrigerator with higher power
- Higher power of 700 MHz RF system for linac
- Arcs with a slightly more sophisticated lattice
- Polarized e-Gun with high current with FEL-driver

At the same time, an electron ring and its high power RF system is not required. In addition, one of the layout linac-ring eRHIC will take advantage of the existing RHIC tunnel, which will reduce it cost significantly. It also provides for significant (3-fold) reduction of the losses for synchrotron radiation, which will save megawatts of the RF power.

Therefore, the overall cost is likely to be close to, or slightly below the ring-ring design.

5. R&D items

Linac-ring eRHIC scheme is based on new emerging technology of high-current energy recovery superconducting RF linacs. Accordingly, there is a significant list of R&D items, the principal issues being

- High current polarized electron gun
  - Cathode material, lifetime and cooling
  - Peak current
  - Relaxation time
  - Average beam current
  - FEL source for the photocathode
- High current superconducting cavity structures
  - Five-cell single mode RF structure
  - Superstructures with HOM damping

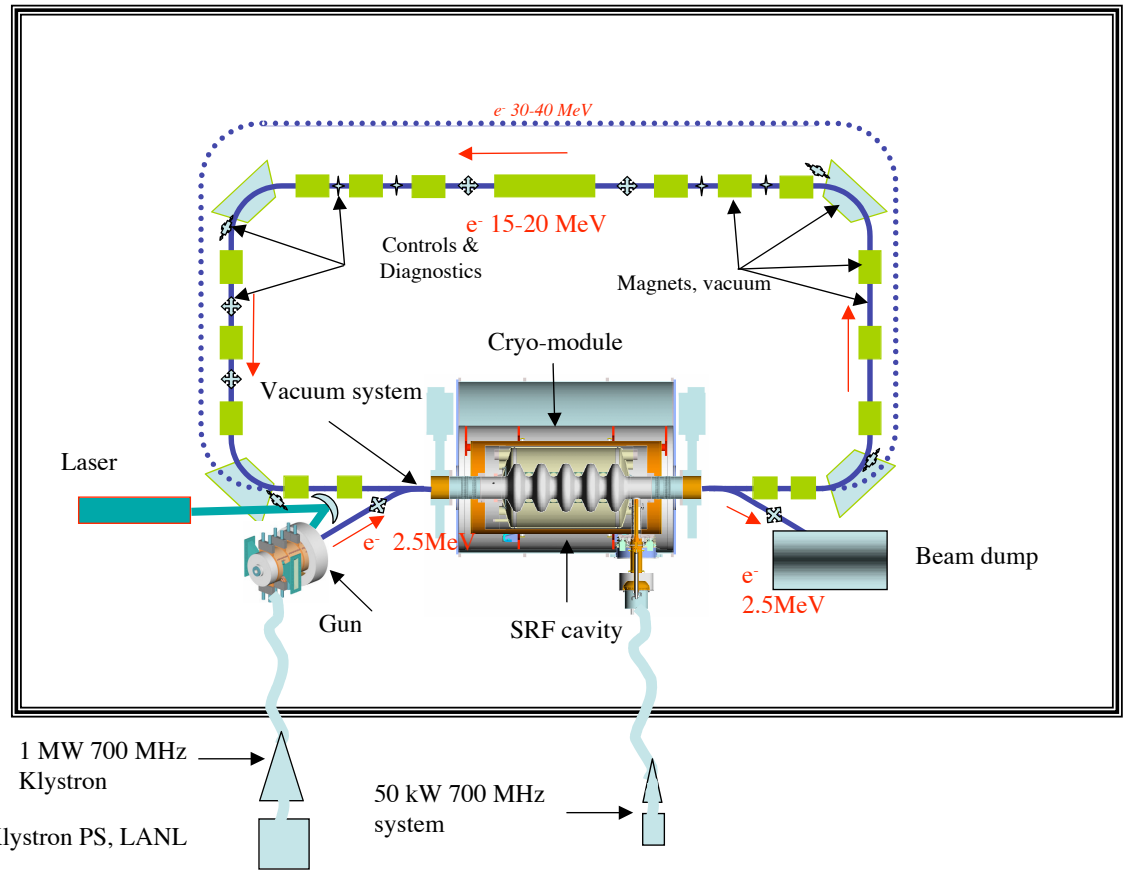

Fig.5.1 Schematic layout of the prototype ERL which is under construction in BNL. This ERL will serve as a test-bed for the concepts of all ERL needed for eRHIC: a) electron cooling, b) FEL for polarized electron gun, and, c) the 10 GeV ERL.

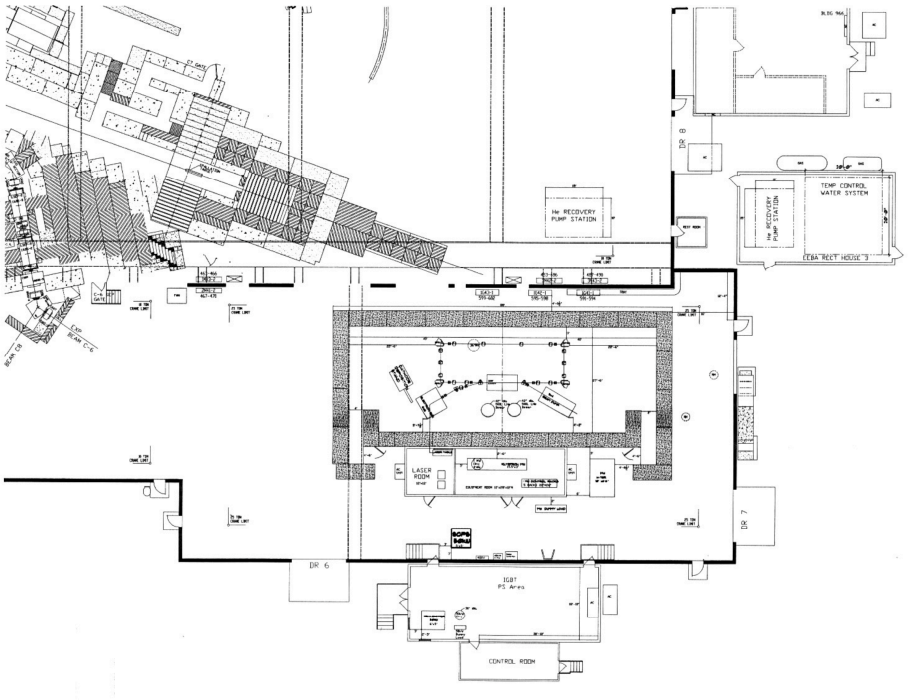

Fig.5.2. Location of the prototype ERL in building 912 at BNL. The experiments are planned to start in mid-2006.

Presently, BNL's accelerator community and others are devoting significant R&D efforts to these issues. They are developing a high-current ERL prototype based on five - cell single-mode SRF structure (planned to be tested in 3-4 years) that will serve as a test bed for both the electron-cooling system and the ERL for eRHIC. In addition, the main centers for SRF technology (Jefferson Laboratory and elsewhere) also are also moving towards developing high-current SRF ERLs. The major technical issues about o the SRF ERL for eRHIC probably will be resolved within 5-10 years. BNL is in excellent position to lead these efforts.

Generating a polarized electron beam with 0.15-0.5 A average current is, and will be, a main R&D item towards the linac-ring eRHIC. Fortunately, an intensive R&D program for linear colliders made several important breakthroughs [5.1-5.3] in such critical areas as surface charge limit and cathode lifetime. Still, there are many problems that must be addressed during feasibility studies for the linac-ring eRHIC. MIT has the relevant expertise to lead these R&D efforts for the eRHIC.

It is also important that polarized electron sources with similar parameters are under development for linear electron-positron colliders [5.3]. Most of beam parameters required for eRHIC electron polarized gun were obtained separately (see Figs 5.3-5), but never in the complete combination. For example, bunches of polarized electrons with charges exceeding by 20-fold that required for the ERL-based eRHIC were demonstrated experimentally (see Figs 5.3), but the duration of the pulses was a few hundreds of nanoseconds [5.2]. Similarly (see Figs 5.4), bunches of polarized electrons with very low normalized emittance were generated [5.4], but with a much smaller charge per bunch.

Therefore, attaining a complete set of parameters requires several very serious developments. Fortunately, many parameters for eRHIC polarized electron gun are close to that of next electron-positron linear collider (see Table 5.1). Therefore, the extensive R&D program for developing such sources for linear colliders [5.5] will address important issues relevant for the ERL-based eRHIC. In any case, developing polarized electron guns is the one of the main R&D for ERL-based eRHIC.

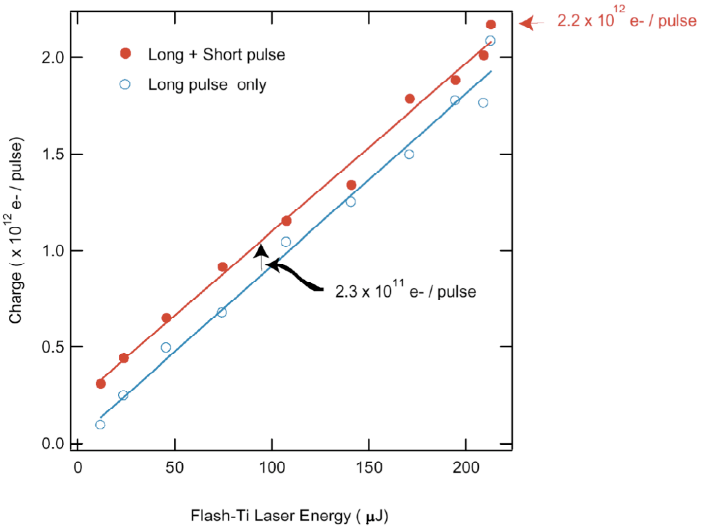

Fig. 5.3. Measured charge per pulse from a ∅14 mm GaAS photocathode [5.2]

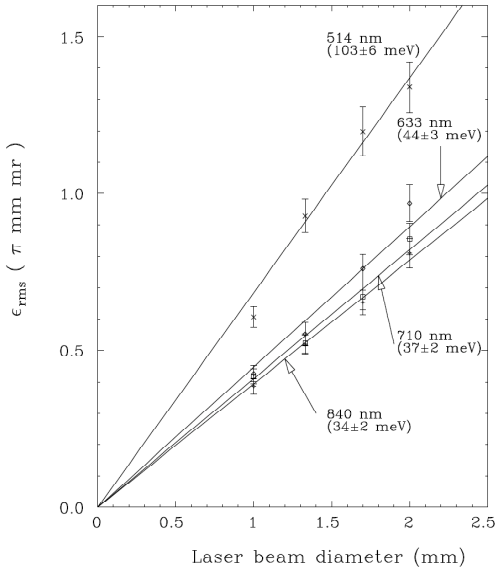

Fig. 5.4. Measured normalized emittance from a polarized e-beam photocathode at CEBAF [5.3]. Simple extrapolation of these measurements to ∅14 mm cathode (i.e., the geometry of the cathode) gives normalized emittance ~ 5 mm x mrad. It supports our assumption that emittance will be dominated by the space-charge effects (see Table 2.1).

Table. 5.1. R&D specifications for polarized electron gun for the next linear collider (a), and for the R&D test gun (b)

	NLC	JLC	TESLA	CLIC
Number of bunches/train	95	95	2820	154
Bunch spacing (ns)	2.8	2.8	337	0.66
DR energy GeV	1.98	1.98	5	1.98
Charge per bunch (nC)	2.56	1.9	3.2	1.0
Injected emittance (mm-mrad)	100	100	10	7
Damped beam emittance (h)	3	2.6	8	.43
Damped beam emittance (v)	0.03	0.004	0.02	0.003
Damped beam bunch length (ps rms)	13.3	16.6	20	10
Damping time (ms)	5.2	3.9	50	21
Damping cycles	4.8	4.8	4	6
Bunch trains per ring	3	3	1	12
Repetition rate (Hz)	120	150	5	100

(a)

Parameter	Symbol	Value	Units
Single Bunch Charge	Q_b	2	nC
Number of Bunches	Nb	1	
Bunch length (FW)	Δt	10	ps
Emittance, normalized	$\gamma\varepsilon$	10	mm-mrad
Energy	E	≈ 5	MeV
Polarization	P	> 80	%
Quantum Efficiency	QE	0.1	%
Repetition Rate	f_{rep}	10	Hertz
Operation Lifetime	τ_{ops}	> 4	Hours

(b)

Smaller but important R&D efforts also will focus on detailed studies and self-consistent simulations of feedback suppressing the kink head-tail instability, the studies of beam-beam effects at low e-beam energies, and the transverse stability of the e-beam in the ERL.

References:

[5.1] P. Hartman et al., "Polarized Electron Linac Sources", In Proc. Of The 2nd eRHIC workshop, Yale, CN, April 6-8, 2000, p.120
T. Zwart et al., "Polarized Electron at Bates: Source to Storage Ring", Proc. Of Second EPIC Workshop, Cambridge, MA, 14-15 September 2000, p.343

[5.2] G. Dugan, "Linear collider: Electron and positron source Potential R&D items", www.lns.cornell.edu/public/LC/MMTI/SourceR&D.pdf

[5.3] ICFA workshop on polarized RF guns for linear colliders, Fermilab, April 18-20, 2001 bc1.lbl.gov/CBP_pages/wim/rfguns_workshop/ RFGuns_workshop.pdf

[5.4] B. M. Dunham, L. S. Cardman, "Emittance Measurements for the Illinois/CEBAF Polarized Electron Source", epaper.kek.jp/p95/ARTICLES/WPC/WPC17.PDF

[5.5] J. Sekutowicz, Proceedings of Linear Accelerators Conference, Tsukuba, Japan, 1994

6. Future energy upgrades and developments

Extending the range of the eRHIC e-beam's energy down to 1 GeV and up or even above 20 GeV is very straight forward with linac-ring eRHIC. It is also for linac-ring eRHIC to have multiple IPs and detectors.

Extending the energy to both into higher and lower range is a natural progression for the ERL-based eRHIC. At low energies, the main problem is the stability of the beams at very high luminosity. An increase in energy principally causes a rise in the intensity of synchrotron radiation in the IP. In principle, an energy of 20-to-25 GeV can be reached in the ERL either by increasing the length of linacs (see Fig.1), or by increase of the number of passes through the system (see Fig.6.1). The most economical choice for the 25 GeV upgrade will be decided by the relative cost of the arcs vs. linac.

Arcs issues

Arcs can be packed on the top of each other for keeping the radii of curvature maximal at all energies[19]. Ultimately, 20+ GeV ERL can utilize RHIC tunnel for the arcs (i.e., maximize the radius of curvature) to keep synchrotron-radiation power under control, i.e. with synchrotron radiation power below ~8 kW/meter presently attained at B-factory.

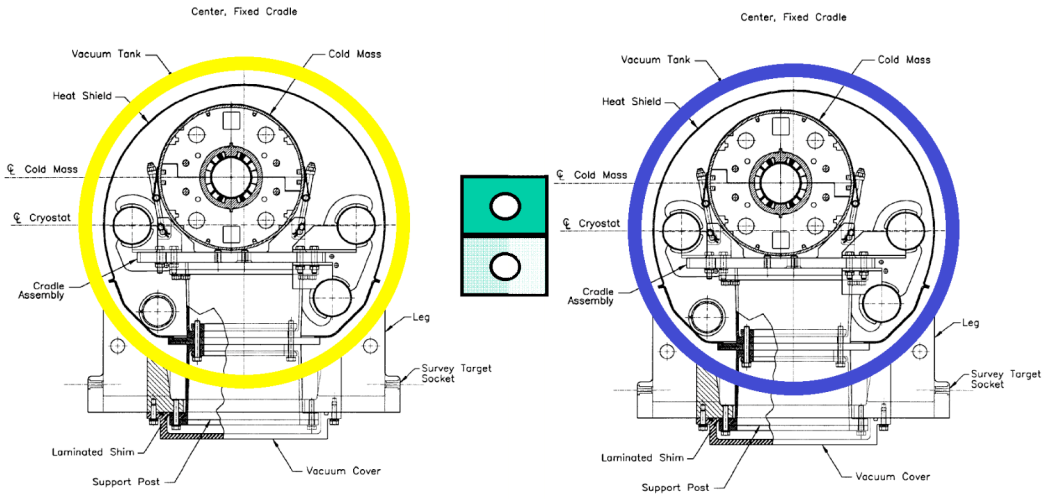

Fig. 6.1. Schematic of the arcs (green rectangle) for the linac-ring eRHIC located in the RHIC tunnel on the top of each other. The nominal number of arcs is two for 20 GeV case, but it can be increased if needed.

Using RHIC tunnel for ERL's arcs significantly increases the radii of curvature and reduces synchrotron radiation losses. Assuming 85% filling factor for the arcs, the 10 GeV ERL will have energy loss of less than 2 MeV per pass and very low linear power

[19] Note that vertical displacements via a dogleg required for this scheme to keep the ERL spin-transparent.

density of synchrotron radiation: 0.22 kW/meter. The linear power density of synchrotron radiation will reach the level of 8.78 kW per meter, which can be considered as attainable, for 25 GeV ERL

IP implications

Increasing electron energy entails growth of the synchrotron-radiation power in the IP. Fortunately, it also reduces the electron beam's emittance and the vertical opening of the synchrotron-radiation fan.

There are two possible solutions for lowering the synchrotron-radiation background in the IP, which are possible only in linac-ring eRHIC:

- First is a further reduction of the ion beam emittance and lowering the electron beam's current (i.e., luminosity stays unchanged)
- Second is to use fewer hadron bunches in RHIC (from 360 to 120*) with the same total intensity of the hadron beam (subject to beam stability studies). This solution reduces the repetition rate of electron bunches, and lowers the synchrotron-radiation background three-fold..
    - This solution has an additional advantage – it is perfectly compatible with present scheme of hadron-hadron collisions; there are no parasitic collisions of hadron beams at both sides of IPs.
    - Additional electron cooling requirements: For the above scheme, an e-cooler is needed with the same average e-beam current but with a three-fold higher charge per bunch.

In addition, ERL created the ideal environment for γ-p, γ-ion and γ-e colliders, where γ-beams with energies up to 10 GeV are generated via Compton backscattering. This scheme is prohibited in the ring-ring scenario.

7. Summary

The linac-ring eRHIC naturally fits with the benefits afforded by electron cooling of ion- and proton-beams in the RHIC. It is based on modern rapidly evolving accelerator technology – energy-recovery superconducting linacs. The ERL's configuration of eRHIC takes advantage of lower ion/proton beam emittance and can reach luminosities above 10^{31} for e-Au, and above 10^{33} for e-p collisions.

First, ERL invariably can be optimized to reach maximal luminosity with present and future parameters of the RHIC beams.

Second, ERL offers significant simplification in the final focus, as well as in detector designs.

Third, the ERL's configuration is always compatible with standard and future RHIC beam intensities, independently of the emittance of the ion and proton beam.

Fourth, the ERL's configuration is ideal for flexible e-beam polarization and energy tunability.

Fifth, the ERL's configuration is upgradeable to higher energies, higher luminosities, and multiple IPs.

Sixth, the ERL's configuration can significantly reduce background synchrotron radiation in the IP region by taking maximum advantage of the lowering of emittance via electron cooling.

In a long run, the ten^{+}-fold higher luminosity (compared with best predicted performance of ring-ring option at top energy), flexibility in the IP design, the full compatibility with RHIC operations, and flexible e-beam energy and polarization are probably most important advantages of the ERL configuration.

8. Acknowledgements

We would like to thank Avril Woodhead and Pamela Manning (both BNL) for their indispensable help with making this document readable.